Journal of Geophysical Research: Oceans

RESEARCH ARTICLE
10.1029/2018JC014511

Seasonality of Freshwater in the East Greenland Current System From 2014 to 2016

Isabela Alexander-Astiz Le Bras[1], Fiamma Straneo[1], James Holte[1], and N Penny Holliday[2]

[1]Scripps Institution of Oceanography, University of California, San Diego, La Jolla, CA, USA, [2]National Oceanography Centre, Southampton, UK

Key Points:
- The East Greenland Current system carries 70% of the freshwater transport across OSNAP East
- Freshwater is mixed from the shelf onto the slope by winter cooling
- Ship-based summer surveys likely underestimate the mean freshwater transport at Cape Farewell

Correspondence to:
I. A.-A. Le Bras,
ilebras@ucsd.edu

Citation:
Le Bras, I. A.-A., Straneo, F., Holte, J., & Holliday, N. P. (2018). Seasonality of freshwater in the East Greenland Current system from 2014 to 2016. *Journal of Geophysical Research: Oceans*, *123*. https://doi.org/10.1029/2018JC014511

Received 29 AUG 2018
Accepted 19 NOV 2018
Accepted article online 22 NOV 2018

Abstract The initial 2 years of Overturning in the Subpolar North Atlantic Program mooring data (2014–2016) provide the first glimpse into the seasonality of freshwater in the complete East Greenland Current system. Using a set of eight moorings southeast of Greenland at 60° N, we find two distinct, persistent velocity cores on the shelf and slope. These are the East Greenland Coastal Current, which carries cold, fresh water from the Arctic and Greenland along the shelf, and the East Greenland/Irminger Current over the slope, which is a combination of cold, fresh waters and warm, salty waters of Atlantic origin. Together, these currents carry 70% of the freshwater transport across the subpolar North Atlantic east of Greenland. The freshwater transport referenced to a salinity of 34.9 is approximately equipartitioned between the coastal current (East Greenland Coastal Current) and the fresh portion of the slope current (East Greenland Current), which carry 42 ± 6 and 32 ± 6 mSv, respectively. The coastal and slope current freshwater transports have staggered seasonality during the observed period, peaking in December and March, respectively, suggesting that summer surveys have underestimated freshwater transport in this region. We find that the continental slope is freshest in the winter, when surface cooling mixes freshwater off the shelf. This previously unmeasured freshwater over the slope is likely to enter the Labrador Sea downstream, where it can impact deep convection.

Plain Language Summary East of Greenland, the ocean has very low salinity, as fresh water and sea ice from the Arctic as well as Greenland melt and icebergs flows into it. This fresh water has the potential to alter the formation of dense water by cooling because it is very light due to its low salinity. This, in turn, is expected to affect global ocean circulation and climate. Despite these potential consequences, the pathways of freshwater around Greenland are uncertain, and measurements outside the summer months are scarce. Here we present the first year-round measurements of the complex current system on the continental shelf and slope southeast of Greenland. We find that the two currents (one on the shelf and one over the slope) have a maximum in freshwater transport in the late fall and winter, respectively. This implies that summer measurements have been underestimating the amount of freshwater these currents carry. We find a freshwater maximum over the slope in winter and present evidence that this freshwater has been mixed off the shelf by winter cooling. This is a novel pathway for freshwater that is likely to have consequences downstream.

1. Introduction

Freshwater is a key player in the formation of globally significant water masses in the subpolar gyre (Manabe & Stouffer, 1995). In particular, the freshwater flowing east of Greenland, which includes Arctic freshwater and sea ice, as well as Greenland melt and icebergs, has been shown to be the primary source of freshwater for the subpolar gyre interior in recent modeling studies (Gillard et al., 2016; Luo et al., 2016; Marson et al., 2018; Schulze Chretien & Frajka-Williams, 2018; Tesdal et al., 2018; Wang et al., 2018). Freshwater export from the Arctic and Greenland is expected to increase (Alley et al., 2005; Wang & Overland, 2009), with potential consequences for the formation of intermediate North Atlantic Deep Waters and global climate. The mechanisms that govern freshwater spreading off the Greenlandic shelf are not well understood, however, and measurements of freshwater in this harsh, remote and often ice riddled region are scarce, particularly outside the summer months.

At Cape Farewell, freshwater flows southward in two velocity cores known collectively as the East Greenland Current (EGC) system. On the shelf, the East Greenland Coastal Current (EGCC) carries cold, fresh water. The

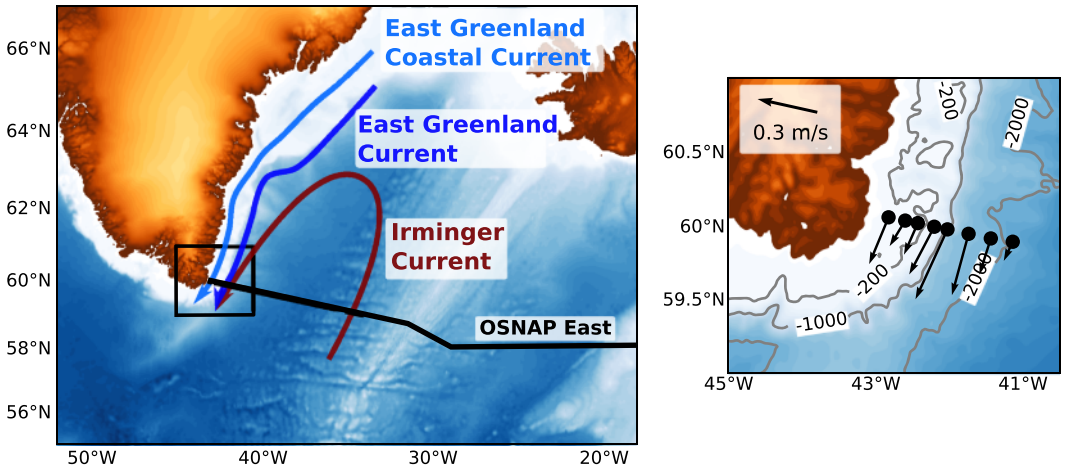

Figure 1. (left) Map of study area with schematic arrows showing the approximate positions of the currents in the East Greenland Current system and the position of the OSNAP East line. The East Greenland Coastal Current flows along the Greenlandic shelf. By Cape Farewell, the East Greenland Current, which originates in the Arctic, and the Irminger Current have merged into one current (East Greenland/Irminger Current). Because their acronyms are easily confused, we refer to the East Greenland Coastal Current as the coastal current and the East Greenland/Irminger Current as the slope current throughout. (right) Inset showing the mean velocity in the top 150 m measured by each mooring from August 2014 to August 2016. The inset position is highlighted with a black square on the map to the left. OSNAP = Overturning in the Subpolar North Atlantic Program.

merged East Greenland/Irminger Current (EGIC) flows over the slope offshore (Figure 1). The EGIC carries both fresh, cold waters that are brought from the Arctic along the shelfbreak by the EGC (Rudels et al., 2005) and warm, salty waters of Atlantic origin delivered by its Irminger Current (IC) component (Lherminier et al., 2010). Yet farther offshore, in the central Irminger Sea, the weakly depth-dependent Irminger gyre flows cyclonically, recirculating waters from the Labrador Sea (Lavender et al., 2005; Spall & Pickart, 2003; Våge et al., 2011). Because our focus is on the full EGC system, and the acronyms EGCC and EGIC are easily confused, we will refer to the EGCC as the coastal current and the EGIC as the slope current throughout.

After rounding the tip of Cape Farewell, these waters flow cyclonically around the Labrador Sea. Along the way, they are diverted into the interior of the subpolar gyre at several locations. Holliday et al. (2007) found a significant retroflection at Cape Farewell: shipboard measurements in the summer of 2005 revealed that 5.1 of the 15.5 Sverdrups (Sv; $\times 10^6$ m^3/s) of volume transport over the slope was diverted into the central Irminger Sea, carrying comparatively fresh water into the interior of the basin. Downstream, west of Greenland, the slope current becomes dynamically unstable due to changes in the steepness of isobaths (Bracco et al., 2008) and sheds Irminger Rings which propagate into the central Labrador Sea (Lilly et al., 2003). Irminger Rings carry warm/salty water of Atlantic origin that restratify the intermediate depths of the Labrador Sea after convection and can have very stratified freshwater caps (de Jong et al., 2014; Rykova et al., 2015).

In general, the shelfbreak is a barrier to the transport of freshwater from the shelf into the ocean interior. This is because oceanic flows conserve Potential Vorticity and the bathymetric gradient of the continental slope gives rise to a large Potential Vorticity gradient. Hence, the water most likely to be diverted offshore at Cape Farewell and in the West Greenland Current is the water that is closest to the interior to begin with, as Schulze Chretien and Frajka-Williams (2018) found in a recent modeling study. In order to spread into the interior, then, water must also be transported off the shelf. Lin et al. (2018) recently demonstrated one mechanism by which this can occur. By examining shipboard measurements from the summer of 2014, they find that the coastal current is diverted offshore west of Cape Farewell as it follows isobaths, facilitating freshwater transport off the shelf there.

Once in the Labrador and Irminger Sea interior, freshwater from the continental shelf and slope can affect water mass formation through convection (Aagaard & Carmack, 1989; Straneo, 2006; Weijer et al., 2012; Yang et al., 2016). The freshwater input increases the stratification and must be cooled more than underlying saltier waters before becoming dense enough to convect. During the Great Salinity Anomaly of 1967–1971, convection was halted by an anomalously large influx of freshwater (Lazier, 1980). These downstream consequences

motivate the quantification of freshwater transport in the EGC system and the identification of mechanisms that export freshwater from the shelf in this work.

Synoptic summer measurements of coastal current volume and freshwater transport range from 0.5 to 2 Sv and 50 to 70 mSv, respectively (Bacon et al., 2002; Lin et al., 2018; Pickart et al., 2005; Sutherland & Pickart, 2008; Wilkinson & Bacon, 2005). Sutherland and Pickart (2008) hypothesized that the coastal current's variability is driven by downwelling-favorable winds, which steepen the freshwater density front on the shelf. There have been no year-round measurements of the transport and properties of the coastal current prior to this study that confirm this link. The only glimpse into the seasonality of the coastal current is from a modeling study (Bacon et al., 2014), which found seasonal peaks in both volume and freshwater transports in February: 3.8 Sv and 106 mSv, respectively.

The origin of the coastal current remains uncertain. A similar feature has been observed north of the Denmark Strait (Havik et al., 2017), and its connectivity south of Denmark Strait is well established (Sutherland & Pickart, 2008; Wilkinson & Bacon, 2005), yet it is unclear if the coastal currents are connected across Denmark Strait. A water mass analysis and laboratory experiments indicate that the coastal current may originate in the Kangerdlugssuaq Trough, just south of the Denmark Strait (Sutherland et al., 2009; Sutherland & Cenedese, 2009). Bacon et al. (2008) suggest that Arctic sea ice is a major source of freshwater for the coastal current; they claim that sea ice is pushed into the coast by the dominant winds and melts into the coastal current as it is advected southward. The significant presence of sea ice melt in the coastal current is supported by $\delta^{18}O$ isotope measurements (Cox et al., 2010).

Just off the shelf, the slope current carries a blend of Polar and Atlantic waters and has a volume transport an order of magnitude larger than the coastal current's. Daniault, Lherminier, et al. (2011) made the most comprehensive year-round measurements of the slope current before this study using a moored array from 2004 to 2006. They estimate a slope current volume transport of 17.3 ± 1.0 Sv and find a significant correlation between the wind stress curl over the Irminger Sea and the slope current volume transport. They hypothesize that this link reflects local gyre spinup in the Irminger Sea. This link was confirmed when Daniault, Mercier, et al. (2011) extended the slope current volume transport estimates to 1992–2009 using satellite altimetry. There are no comprehensive year-round measurements of salinity in the slope current; however, therefore, the seasonal variability of its freshwater transport is unknown.

In this study, we use the first year-round observations of the full EGC system to quantify its freshwater transport and variability, providing an updated view of this region upstream of globally significant convection sites. The observational data set consists of eight moorings which were deployed on the shelf and slope southeast of Greenland at 60° N as part of Overturning in the Subpolar North Atlantic Program (OSNAP) from 2014 to 2016 (Holliday et al., 2018; Li et al., 2017; Lozier et al., 2017). We find that the coastal and slope current freshwater transports have staggered peaks in the late fall and winter, respectively. They carry similar amounts of the freshwater fresher than the reference salinity (34.9) at their peaks. This implies that freshwater transports in this region have been underestimated by summer measurements: the coastal current freshwater transport almost doubles from June to December, and the fresh portion of the slope current freshwater transport quadruples from August to February. We find that the water over the slope is freshest in the winter and identify a potential mechanism for mixing freshwater off the shelf.

First, we describe the data processing and transport analysis procedures (section 2). In the results section, we report on the coastal and slope current transports individually before detailing the seasonal evolution of freshwater in the joint system (section 3). In particular, we describe a previously undocumented winter freshwater maximum over the slope and diagnose potential drivers of transport variability. Finally, we discuss the context and implications of the observed seasonality in freshwater transport in the EGC system (section 4).

2. Methods

2.1. Data

We present measurements from the eight westernmost moorings of the OSNAP East line: seven U.S. OSNAP Cape Farewell (CF) moorings and one U.K. OSNAP mooring (M1) which spanned the shelf and slope southeast of Greenland at 60° N from 17 August 2014 to 28 July 2016 (Figures 1 and 2). Velocity was measured directly by a combination of point current meters recording every 30 min and Acoustic Doppler Current Profilers (ADCPs) returning hourly data. Instrument accuracy is estimated at ± 0.01 m/s. Each instrument's velocity record was low-pass filtered with a 40-day cutoff to remove tides and was then decimated to daily values.

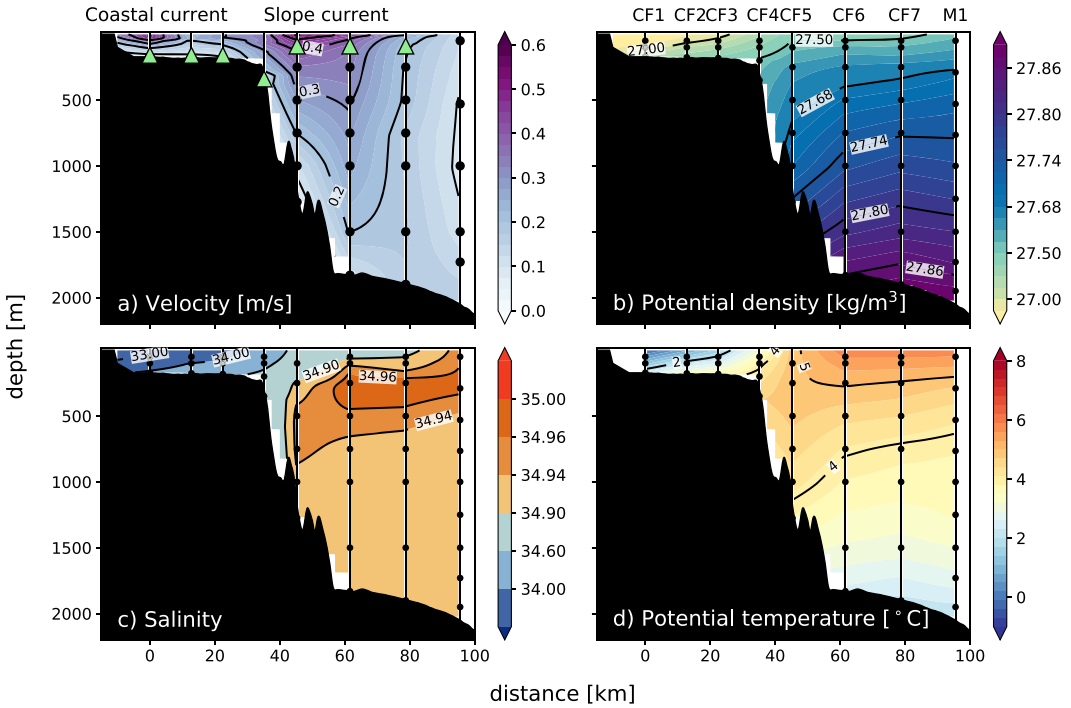

Figure 2. Time mean sections of (a) along-stream velocity, (b) potential density, (c) salinity, and (d) potential temperature based on the OSNAP Cape Farewell (CF) mooring data from August 2014 to August 2016. (a) Green triangles indicate upward-looking Acoustic Doppler Current Profilers and black circles current meters. (b–d) Black circles indicate microcats, which measure salinity, temperature, and pressure. The coastal current (East Greenland Coastal Current) is apparent on the shelf, measured by CF1-CF2, while the slope current (East Greenland/Irminger Current) is offshore, from CF2-M1. The unmeasured portion of the shelf is filled in by extrapolating daily fields of salinity and density horizontally and using geostrophy to calculate the velocity.

Temperature and salinity (T/S) were derived from SBE37 microcat CTDs recording every 15 min (Figure 2). The initial microcat precision is ±0.002 °C for temperature and ±0.0003 S/m for conductivity, which translates to ±0.0001–0.005 in salinity and for a temperature range of 0–8 °C. Microcat conductivity measurements are known to experience significant drift. Upon recovery, the moored microcats were calibrated by comparing their measurements to shipboard lowered CTD measurements, as described in Kanzow et al. (2006). These comparative data were obtained through calibration casts; the moored instruments were attached to the shipboard CTD rosette, and during each cast, the rosette halted for approximately 5 min at five prescribed pressures to allow the microcats to equilibrate. Additional salinity drifts were removed from the 100- and 400-m instrument data on moorings CF4 and from the 100-m instrument on CF6 with the guidance of Seabird technical staff. Post calibration of T/S data, they were averaged to daily mean values.

All daily-averaged data (velocity, temperature, and salinity) were interpolated linearly to 2-db bins in the vertical using the pressure measured by the instruments. Upward-looking ADCPs measured velocity near the surface at all CF moorings. The topmost ADCP bin was generally at 20 m, but the depth of the shallowest bin was affected by blowdown at moorings CF4–CF7. The shallowest current meter at M1 was at 50 m. At each mooring, the shallowest velocity measurement was extrapolated to the surface each day. T/S were extrapolated to the surface using the gradient between the two shallowest measurements available at each mooring and day. This extrapolation method was found to better agree with full-depth shipboard CTD measurements than extrapolating the surface-most value. Even using this method, the tendency was for the surface gradients of T/S to be underestimated in summer. The shallowest T/S measurements were generally at about 50 m, but the moorings experienced blowdowns by the currents, usually several tens of meters, but up to 200 m in the daily average at CF5 in the winter, where the flow was the strongest.

Data return was excellent, with the exception of several shallow instruments. RBR XR-420s were deployed at 50 m on CF5 and CF7: the CF5 instrument was lost, and the CF7 instrument returned about 1 year of data. The onshore-most mooring (CF1) lost flotation progressively starting in May 2015, likely due to iceberg col-

lisions. The 50-db instrument fell on 17 May 2015 when the weak link connecting it to a panther float was broken, and the 100-db instrument fell when the intermediate flotation was flooded on 14 August 2015. The bottom tripod-mounted ADCP measured velocity throughout the water column for the full deployment, but after August 2015, the only reliable T/S measurements were at the bottom (170 m). T/S were reconstructed using the difference between the bottommost measurements and each instrument's measurements before it lost flotation. The velocity in the full water column evolved similarly both years, lending support for using the first year of data to inform the reconstruction of the second. To reconstruct temperature, the constant mean difference was added to the bottommost measurement, while for salinity, a monthly mean value was used, interpolating linearly where necessary. Because the shelf is stratified by salinity, the seasonal evolution of stratification is taken into account using this method. Pressure was filled with the constant mean pressure recorded by each instrument before it lost flotation. Because the CF1 salinity data in the second year was reconstructed from bottom values, our analysis of freshwater transport seasonality in section 3.3 focuses on the first year of data. We present the full-length freshwater transport time series incorporating the reconstructed values and use both years to calculate the mean freshwater transport.

The wind stress data used are the ERA5 product from the European Centre for Medium-Range Weather Forecasts with approximately 30-km resolution (Dee et al., 2011), generated using Copernicus Climate Change Service Information (2018). ERA5 does include sea ice which is taken into account when calculating wind stress. Monthly sea ice concentration data with a spatial resolution of 25 km derived from passive microwave brightness temperature data was downloaded from the National Snow and Ice Data Center (http://nsidc.org/data/nsidc-0051). Shelf sea ice concentration was determined by averaging between 60–61° N and 42.5–43° W.

2.2. Transport Analyses

All reported transports are in an along-stream coordinate system, where along-stream flow is 203.3° clockwise from North. This angle is the principle axis of the flow in the top 500 m at CF5, which is in the center of the slope current. This is 5° away from the principal axis of the coastal current at CF1 (198.4°). The variance ellipse at CF1 is not as well-defined, however. We define the positive along-flow direction in this south-southwestward direction, so that volume transports have a positive sign.

Freshwater transport is given by

$$FWT = \int\int v(x,z)\left(\frac{S_{\text{ref}} - S(x,z)}{S_{\text{ref}}}\right) \mathrm{d}x\mathrm{d}z, \tag{1}$$

where z is the vertical coordinate, x is the along-mooring array coordinate, v is the along-stream velocity, and S is salinity. We use a reference salinity, S_{ref}, of 34.9. In our coordinate system, a positive freshwater transport results from south-southwestward flow of water fresher than the reference salinity.

Note that the freshwater transport we report cannot be thought of as a component of a salinity budget as mass is not conserved across this partial array (Bacon et al., 2015; Tsubouchi et al., 2012). These observations form a portion of the full cross-basin OSNAP line across which mass is conserved, yet these are only available for the initial 21-month period for which the full OSNAP line data have been processed, 3 months less than the portion we report on here. In comparing with other freshwater transport estimates, we will clarify the impact of the reference salinity. We also place the EGC system observations in the context of the first 21 months of the full OSNAP array in section 3. The reference salinity of 34.9 is commonly used in this region (de Steur et al., 2009) and marks the separation between water of polar and Atlantic origin, so that the freshwater transport can be thought of as indicating the relative influence of waters of polar and Atlantic origins at the array. In our observations, 34.9 highlights the transition between predominantly salinity-stratified and temperature-stratified waters.

The coastal current is defined as all transport inshore of CF2 (Figure 2). The coastal current was measured consistently by the inshore-most mooring, CF1. There is a minimum in velocity magnitude at CF2 in the mean, and this is the median position of the minimum in speed between the coastal and slope currents. As there is no seasonality in the position of the coastal current as measured by the array (13 km between CF1 and CF2), we use CF2 as the static boundary between the coastal and slope currents. Attempts to define a moving boundary between the currents led to noise and no additional insight.

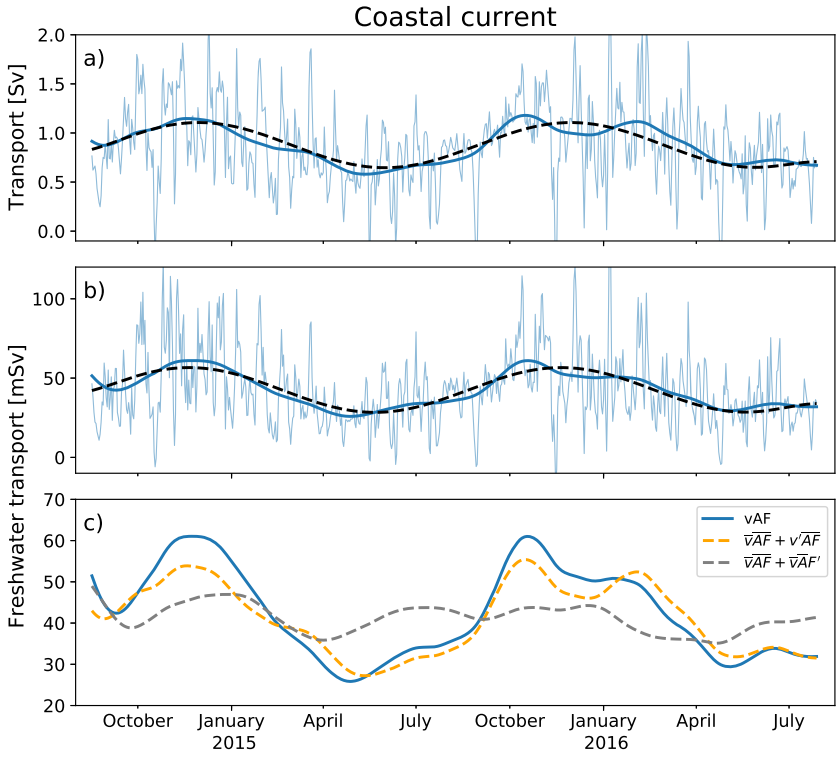

Figure 3. Coastal current (a) volume transport and (b) freshwater transport (referenced to 34.9) from August 2014 to August 2016. The coastal current is defined as all flow inshore of CF2. (a and b) Thin blue lines are daily values, bold blue lines are low-pass filtered with a 50-day cutoff frequency, and black-dashed lines are the seasonal fit. (c) Decomposition of the coastal current freshwater transport variability as defined in section 2.2. The bold blue line is repeated from (b), the variability due to changes in velocity are in orange, and variability due to changes in salinity are in gray.

The inshore edge of the coastal current is not resolved by the moored array, so we approximate the contribution from the remaining shelf area by extrapolating the daily salinity and density fields horizontally for a further 10 km to the continent, using the horizontal gradient between CF2 and CF1. To estimate the along-stream velocity inshore of CF1, geostrophic shear is calculated from the density field, and the absolute velocity is referenced to the bottommost measurement at CF1 for continuity. We discuss the sampling error in our coastal current transport estimate using a comparison to shipboard data in Appendix A.

The slope current is defined as all along-stream flow offshore of CF2 and above the 27.8-kg/m^3 isopycnal, which marks the boundary with the Deep Western Boundary Current (Figure 2; Bacon & Saunders, 2010). Note that this definition includes intermediate water masses (Labrador Sea Water and Irminger Sea Water) which are generally lighter than 27.8 kg/m^3.

All transports are calculated using gridded fields of velocity and salinity, interpolated linearly in the horizontal to include three additional gridpoints between moorings or 2.5-km resolution when extrapolating on the shelf. We interpolate between bottommost observations to fill in properties along sloped bathymetry.

Both daily- and low-pass-filtered transports are shown throughout. We use a second-order low-pass digital Butterworth filter applied in both directions, with a 50-day cutoff frequency. In our analysis of the wind stress forcing in section 3.5, the same form of Butterworth filter is applied to low-pass filter the transport and wind stress (curl) time series with a 5-day cutoff. To diagnose the degree of seasonality in our transport time series, we fit a sine function with a 365.25-day period to the 50-day low-pass-filtered time series. When the correlation coefficient between filtered time series and sine function is 0.85 or greater, the transport time series is deemed to have strong seasonality, and the seasonal minima and maxima of the sinusoidal fit are reported.

Reported uncertainty in all mean transports is a 95% confidence interval using the Student's *t* test with 90 effective degrees of freedom. The degrees of freedom were estimated using an integral time scale found by integrating the autocorrelation function of each transport time series until it reached an initial limit, which was about 8 days for all time series. The degrees of freedom in the correlation between the wind stress and

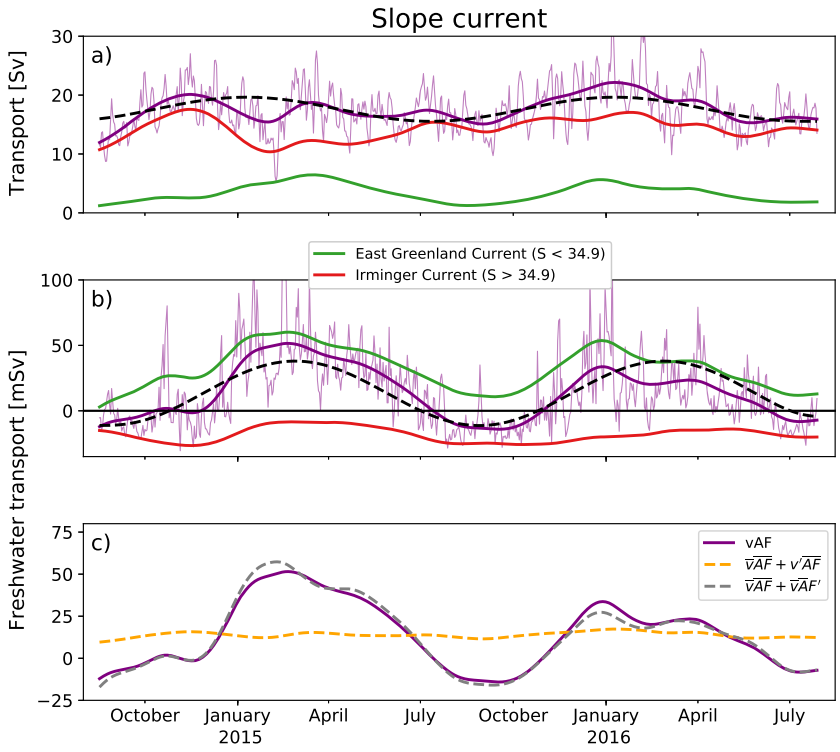

Figure 4. Slope current (a) volume transport and (b) freshwater transport (referenced to 34.9) from August 2014 to August 2016. (a and b) Purple lines show time series for the slope current defined as between CF2 and M1 and above the σ_0 27.8-kg/m^3 isopycnal. Thin purple lines are daily values, while bold purple lines are low-pass filtered with a 50-day cutoff frequency. Green lines indicate the portion of the slope current fresher than 34.9, likely stemming from the Arctic East Greenland Current, while red lines denote the portion saltier than 34.9, likely stemming from the Atlantic Irminger Current. The black-dashed lines show the seasonal fit to each transport time series. (c) Decomposition of the slope current freshwater transport variability as defined in section 2.2. The bold purple line is repeated from (b), the variability due to changes in velocity are in orange, and variability due to changes in salinity are in gray.

volume transports were found in the same way and resulted in an estimate of 10 days (70 effective degrees of freedom), as these time series were low-pass filtered with a 5-day cutoff. The significance of the correlation between the wind stress and volume transport was calculated using the False Discovery Rate (FDR) method (Wilks, 2016) with an allowable FDR of 10% ($\alpha_{FDR} = 0.1$). Our implementation of this method will be detailed in section 3.5.

The contributions of velocity and salinity to the variability of the freshwater transport are diagnosed by doing a Reynolds decomposition of the freshwater transport term (Figures 3c and 4c). For each day, the freshwater transport is vAF, where v is the mean transport in the current, A is its area, and $F = (S_{ref} - S)/S_{ref}$, where S is the mean salinity in the current. The full freshwater transport can be decomposed each day as

$$vAF = (\bar{v} + v')(\bar{A} + A')(\bar{F} + F'), \tag{2}$$

where overlines denote a time mean over the full record, and primes denotes a deviation from that mean. For the coastal current, $A' = 0$ as its extent is fixed, and for the slope current, terms including A' are negligible. For both currents, terms which include the product of two deviation terms are small. This leaves

$$vAF \approx \bar{v}\,\bar{A}\,\bar{F} + v'\,\bar{A}\,\bar{F} + \bar{v}\,\bar{A}\,F'. \tag{3}$$

3. Results

The mean velocity measured by the OSNAP CF array shows the coastal current (EGCC) on the shelf and the slope current (EGIC) over the continental slope offshore (Figure 2). The slope current (EGIC) is a combination of EGC water of polar origin and IC water of Atlantic origin. The wedge of warm, salty Atlantic origin water

Table 1
Summary of Volume and Freshwater Transports Referenced to 34.9 in the East Greenland Current System

		Coastal current (EGCC)	Slope current (EGIC)	EGC portion	IC portion
Volume transport (Sv)	Mean	0.86 ± 0.10	18 ± 1	3.5 ± 0.5	14.3 ± 0.8
	seasonal range	0.64 to 1.1		1.4 to 5.2	
		June/December		August/February	
Freshwater transport (mSv)	Mean	42 ± 6	14 ± 7	32 ± 6	−17 ± 1
	seasonal range	28 to 57	−11 to 38	12 to 51	−25 to −12
		June/December	September/March	August/February	October/April

Note. Mean transports are quoted with their uncertainty (section 2.2). Seasonality is diagnosed by fitting a sine function with a 365.25-day period to the 50-day low-pass-filtered time series (Figures 3 and 4). The seasonal range is the minimum and maximum of the sine function, listed above the month in which they occur. Seasonal ranges are only reported when the correlation between the filtered time series and sinusoidal fit is 0.85 or greater. EGCC = East Greenland Coastal Current; EGIC = East Greenland/Irminger Current; EGC = East Greenland Current; IC = Irminger Current.

is apparent in mean sections from about 100–500 m on the continental slope. The 34.9 reference salinity isohaline bisects the slope current.

Mean transports and their seasonal ranges for all currents and their components are quoted in Table 1, as defined in section 2.2. To place the freshwater transport across our section into the context of the eastern subpolar gyre, we additionally calculated the freshwater transport relative to the full OSNAP East array. The OSNAP East data are complete for the first 21 months of our deployment, and the mean salinity across the entire section (from Greenland to Scotland) was estimated to be 34.9682. Using this salinity as a reference for the freshwater transport across our section during the first 21 months, we find a freshwater transport of 96 mSv across our section, which is 70% of the total freshwater transport across OSNAP East during this time (140 mSv).

In the remainder of this section, we report on the volume and freshwater transports of the coastal and slope currents for the full record, discuss their water mass transformations, and diagnose potential sources of transport variability.

3.1. Coastal Current

The mean volume transport in the coastal current is 0.86 ± 0.10 Sv, and its mean freshwater transport is 42 ± 6 mSv (Table 1). The coastal current volume and freshwater transports display similar seasonality, with seasonal maxima in December and minima in June. Volume transports increase by 72% over the seasonal cycle and freshwater transports by 100% (Table 1), indicating the degree to which coastal current transports may be underestimated by summer observations. A decomposition of the freshwater transport into the contributions from velocity and salinity variability shows that the seasonality in freshwater transport is dominated by variability in the velocity field (Figure 3c).

Historical summertime estimates of the coastal current volume transports span 0.5–2.0 Sv (Bacon et al., 2002; Pickart et al., 2005; Sutherland & Pickart, 2008; Wilkinson & Bacon, 2005). Sutherland and Pickart (2008) estimated 50–70 mSv of freshwater transport (referenced to 34.8) in the coastal current at CF in summer 2004. The most recent estimates, calculated from shipboard data during the OSNAP deployment cruise in August 2014 are 1.0/1.09 Sv of volume transport and 40.95/68.45 mSv of freshwater transport (referenced to 34.8), where the larger estimates are for a section just upstream of the moored array that covered a larger portion of the shelf (Lin et al., 2018). Note that previous studies use reference salinities ranging from 34.8 to 35, but such changes do not impact our coastal current freshwater transport estimates by more than 4 mSv.

Shipboard estimates are consistently larger than our summer estimates from the moored array, and we show a detailed comparison to shipboard observations in Appendix A. We find that the moored array underestimates coastal current volume transports because the narrow velocity core is not always located at the CF1 mooring. The freshwater transport is additionally underestimated in late summer because the moorings do not measure the near-surface freshwater lens. As the coastal current's seasonality is dominated by velocity variability; however, the observed patterns of variability are robust (see Appendix A for additional details).

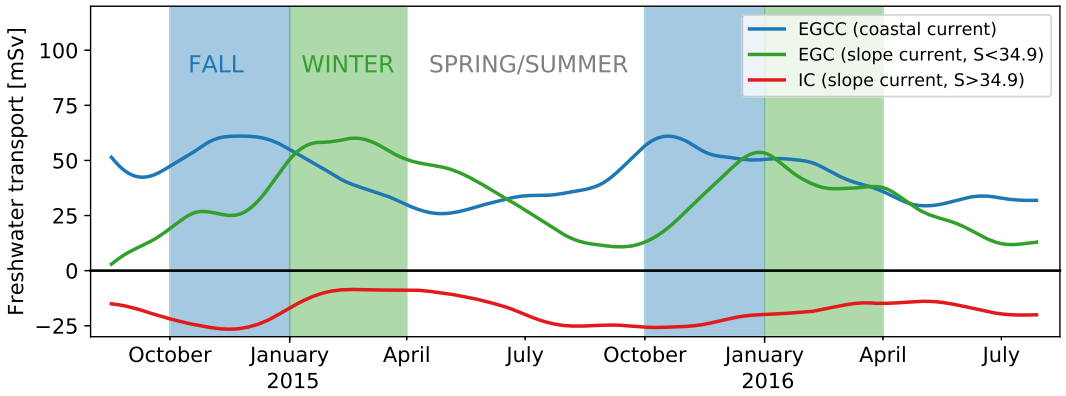

Figure 5. Coastal and slope current freshwater transports. The coastal current freshwater transport is indicated by the thick blue line. The slope current freshwater transport is partitioned into the water fresher than the reference salinity, 34.9, in green and saltier in red. The peaks in freshwater flux in the coastal current and slope currents are staggered, peaking in late fall and winter, respectively. The three labeled periods during the first year of measurement, when salinity measurements on the shelf are more complete, are the focus of Figures 6–9. EGCC = East Greenland Coastal Current; EGIC = East Greenland/Irminger Current; IC = Irminger Current.

Bacon et al. (2014) made the only other estimate of coastal current transport outside of the summer using a coupled ice-ocean general circulation model. They find a seasonal peak in the volume and liquid freshwater transport in February of 3.8 Sv and 90 mSv (referenced to 35.0), respectively. The covariability of the volume and freshwater transport seasonality is consistent between our studies; however, their seasonal transport peaks are both later and larger than those we find. Their estimate is farther north at 63° N, where the shelf is narrower and steeper, which could impact their definition of the coastal current and hence explain the differences in our results. Our observed seasonality is also based on just 2 years of measurements, with complete measurements on the shelf in the first year only, while Bacon et al. (2014) average model output over 8 years. Future measurements will clarify this connection further.

3.2. Slope Current

The slope current's mean volume transport above the σ_0 27.8-kg/m^3 isopycnal is 18 ± 1 Sv, with a standard deviation of 4 Sv. Our sinusoidal fit analysis showed that the slope current's volume transport does not have pronounced regular seasonality (section 2.2 and Figure 4). Our slope current volume transport is comparable to a previous estimate by Daniault, Lherminier, et al. (2011) who measured its velocity with a set of five moorings from 2004 to 2006, they measured 17.3 ± 1.0 Sv with a standard deviation of 3.8 Sv. Note that their offshore-most mooring did not reach the 2,000-m isobath, which likely explains why our estimate is larger.

Historical measurements of slope current volume transport from hydrography, reviewed in Sarafanov et al. (2012), range from 12 to 34 Sv. Sarafanov et al. (2012) find a mean slope current transport of 21.8 ± 4.3 Sv by combining summer hydrographic and satellite altimetry data from 2002 to 2008. Their slope current is defined as the transport at 59.5° N out to 40° W and above the 27.8-kg/m^3 isopycnal. Rossby et al. (2017) use the same definition and calculate a mean slope current transport of 26.9 ± 1.9 Sv from 2012 to 2016 ship of opportunity ADCP measurements. These values are larger than ours and Daniault, Lherminier, et al.'s (2011) as they use a larger extent to define the slope current, pointing to the importance of defining current extent in this region. This is to be expected because the Irminger gyre recirculation flows in the same direction as the slope current throughout the western Irminger Basin (Lavender et al., 2005; Våge et al., 2011).

These measurements give the first glimpse into the seasonality of the freshwater transport on the continental slope at Cape Farewell. The mean slope current freshwater transport is 14 ± 7 mSv. Despite the lack of clear seasonality in the volume transport, shifts in the salinity field on the continental slope cause a striking seasonality to emerge, with a seasonal range from −11 to 38 mSv, peaking in March (Figure 4b and Table 1). As implied by the weaker seasonality in slope current volume transport, the seasonality in slope current freshwater transport is dominated by changes in the salinity structure (Figure 4c).

The slope current can be separated into its EGC and IC components, which are nominally of polar and Atlantic origin, respectively. For consistency and simplicity, we use our reference salinity, 34.9, to separate the EGC and IC components of the slope current, as was done in Pickart et al. (2005). Though the EGC component

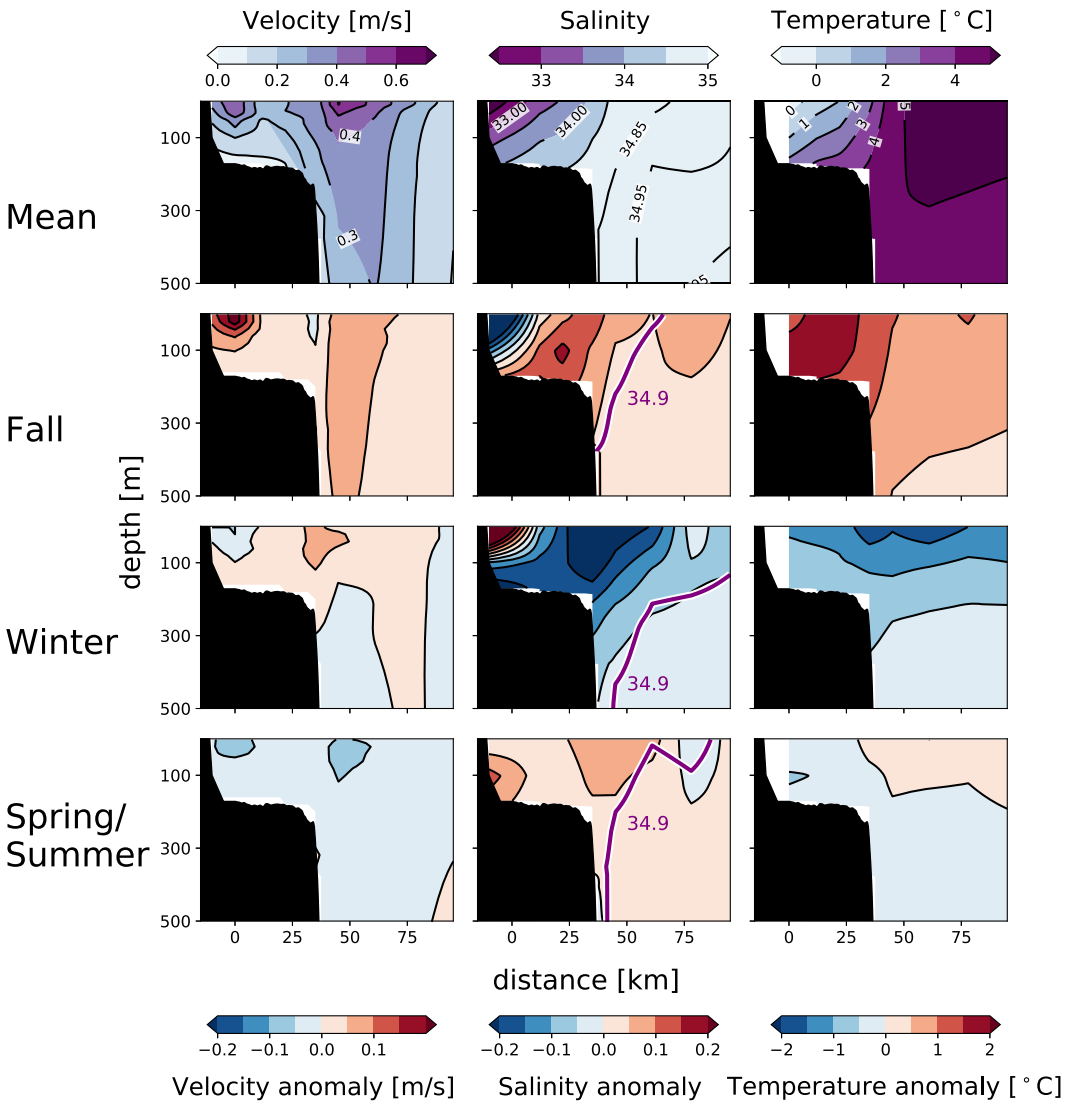

Figure 6. Velocity (left), salinity (center), and potential temperature (right) annual mean (top row) and anomalies (lower panels) during the first full year. Seasons are defined as in Figure 5. Velocity and salinity anomalies are contoured in black every 0.05 of their respective units. Temperature anomalies are contoured every 0.5 °C. Red indicates faster than mean equatorward velocities, saltier water, and warmer temperatures. The 34.9 isohaline is overlain in the salinity anomaly panels in purple. Note that only the top 500 m are shown.

carries a smaller portion of the volume transport than the IC component, it makes a larger contribution to the freshwater transport of the slope current (Figure 4b). This is because it includes waters much fresher than the reference salinity, while the IC component carries waters only marginally saltier than the reference salinity.

We find that the IC component of the slope current has a mean volume transport of 14.3 ± 0.7 Sv and the EGC component a mean transport of 3.7 ± 0.5 Sv. Pickart et al. (2005) found the breakdown to be 12.9 Sv in the IC and 0.7 Sv in the EGC from one summer snapshot. Our July–August mean breakdown is 14.6 Sv in the IC and the 1.7 Sv in the EGC, which is closer to the proportions that Pickart et al. (2005) found as the EGC component of the slope current peaks outside of summer.

Unlike the coastal current's freshwater transport, the reference salinity used impacts the size and even sign of the slope current's freshwater transport. This is because the slope current includes waters both fresher and saltier than the reference salinity, while all waters in the coastal current are significantly fresher than the reference salinity. However, the seasonal shifts in freshwater transport we discuss here persist regardless of the reference salinity: the slope current is saltiest in the summer/spring and freshest in the winter.

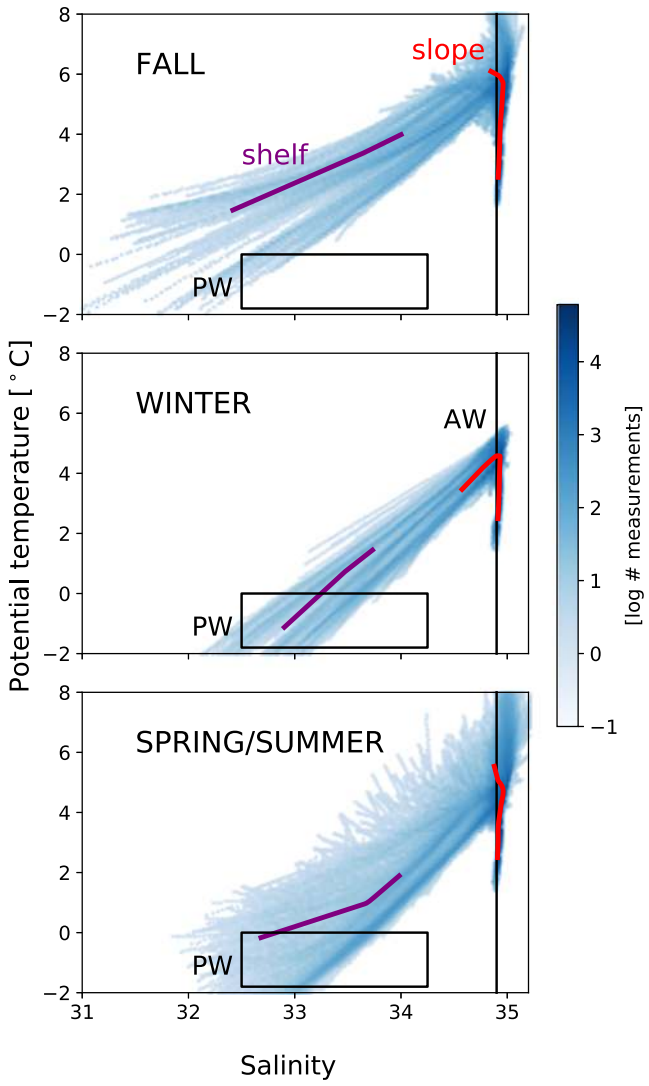

Figure 7. Potential temperature and salinity (T/S) during the periods denoted in Figure 5 in the first year of measurements. Shade of blue indicates the log of the number of measurements in a particular T/S bin, as defined in the legend. Season-mean shelf T/S properties (inshore of CF2) are shown in purple and season-mean slope properties (CF5-6) in red. The 34.9 reference isohaline is denoted by the vertical black line in all panels; the black rectangle shows the standard definition of PW (Harden et al., 2014). AW is highlighted in the winter panel, when mixing between the PW and AW endmembers is apparent. PW = Polar Water; AW = Atlantic Water.

3.3. Freshwater Transport Seasonality in the Full System

The freshwater transport in the coastal and slope currents have staggered seasonality; the coastal current freshwater transport peaks before the freshwater transport in the EGC portion of the slope current (fresher than 34.9) in both measurement years (Figure 5 and Table 1). Our sinusoidal fit analysis places the coastal current's freshwater transport peak in December (57 mSv) and the fresh portion of the slope current's peaks in February (51 mSv). Notably, the coastal current and the fresh portion of the slope current (the EGC) carry roughly equal amounts of freshwater, particularly at their peaks.

The seasonal patterns of freshwater transport can be understood by considering the velocity and property anomaly distributions in the joint shelf-slope system in the first year of measurements (Figure 6). In the fall, the coastal current is the fastest, and the shelf is the freshest (Figure 6), combining to form the fall maximum in coastal current freshwater transport. The fresh anomaly on the shelf is also apparent in T/S space; the freshest water is observed on the shelf in fall (Figure 7). From our time series analysis, we know that the peak in velocity is the dominant factor in determining the coastal current's freshwater transport seasonality, not changes in salinity (Figure 3c). The shelf undergoes seasonal heating and cooling, with the warmest temperatures observed in the fall (Figure 6). This heating pattern is consistent with climatological large-scale patterns of seasonal warming on the shelf, generally observed at the mouth of and within Greenland's glacial fjords several months prior (Straneo et al., 2010). The isohalines are the steepest on the shelf in fall and the horizontal salinity gradient is the largest (Figure 6). As isohalines are equivalent to isopycnals on the shelf, this is consistent with a stronger geostrophic velocity in fall. Offshore, the saltiest water is found in fall, and there is a fast anomaly in the slope current, accounting for the rough anticorrelation between the salty IC component of the slope current's freshwater transport and the coastal current's (Figure 5).

In winter, the horizontal salinity gradients on the shelf decrease, and there is a striking freshwater anomaly centered on the shelf break (Figure 6) which causes the peak in slope current freshwater transport. There is also a fast anomaly in the freshest portion of the slope current, as well as a cold anomaly centered at the shelfbreak (Figure 6). The vertical dipole in salinity anomalies on the shelf indicates that there has been a redistribution of salt in the water column, that is, fresher surface water has been mixed down into the water column by surface cooling. The dipole could also indicate a lateral redistribution, though the mechanism by which this would occur is unclear as the strong northerly winds in the fall and winter cause an Ekman transport toward the coast. We explore the striking freshening over the slope further in section 3.4.

Finally, in the spring and summer months, both currents are the weakest (Figure 6). Water mass properties are generally saltier and cooler than the mean, though the surface waters offshore of the shelfbreak are warmer than the mean.

3.4. Freshwater Over the Slope

Considering properties in T/S space across the full moored array provides some insight into the anomalously fresh properties observed over the slope in winter. The properties over the slope are of particular interest because they are more likely than those on the shelf to be exported into the Labrador Sea, where they can affect deep convection (Schulze Chretien & Frajka-Williams, 2018). As discussed in section 1, the shelfbreak presents a barrier to waters crossing into the interior, even at downstream locations where waters are known to be diverted from the boundary.

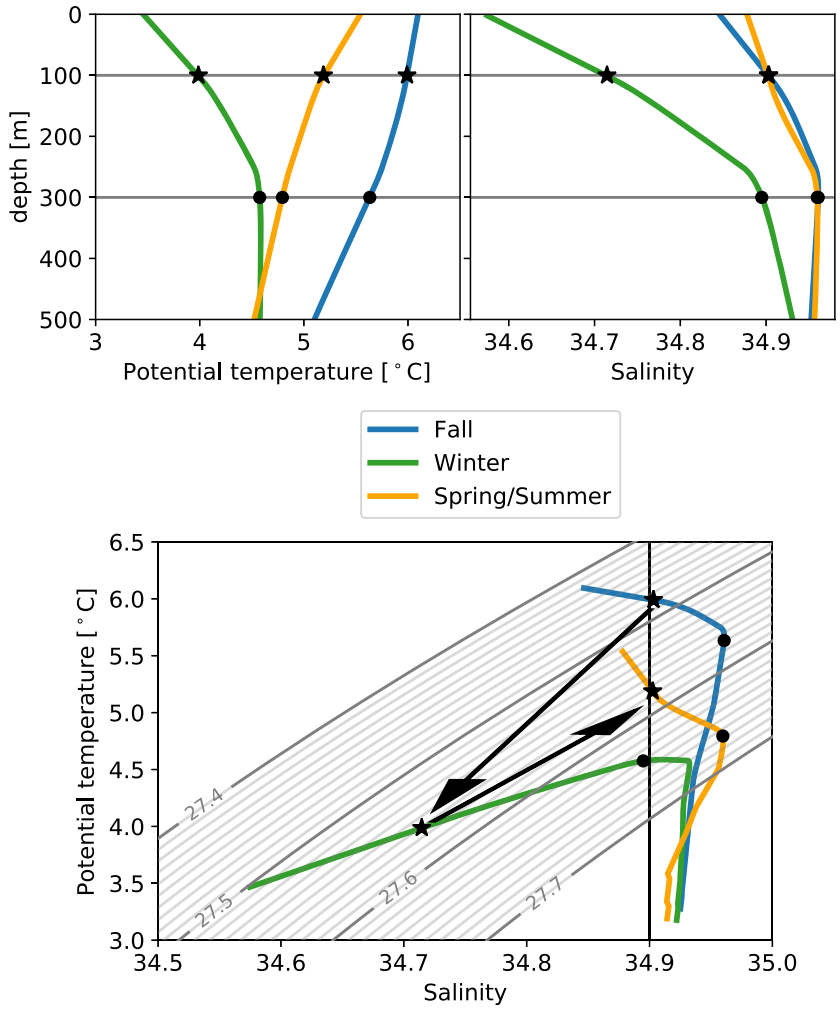

Figure 8. Mean temperature and salinity in the core of the slope current (CF5-6) during the three periods denoted in Figure 5 in the first year of measurements. (top row) Potential temperature and salinity profiles in the top 500 m. (bottom) Temperature and salinity diagram showing the mean properties over the slope (i.e., the red lines in Figure 7). Gray lines indicate isopycnals (referenced to the surface). Temperature and salinity properties at 100 and 300 m are highlighted with black stars and dots, respectively. Water mass changes at 100 m are highlighted by black arrows.

Both T/S play a significant role in determining density in this data set. On the shelf, the water column is salinity stratified. Cold and fresh water sits atop warmer, saltier water, crossing density contours horizontally in T/S space (Figure 7). Water over the slope is generally temperature stratified, crossing density contours vertically on the salty edge of T/S space. The 34.9 isohaline separates these polar and Atlantic regimes effectively.

This transition is particularly striking in the winter, when the warm surface layers apparent in the fall, summer, and spring are absent. In winter, T/S space is dominated by mixing lines between Polar Water and Atlantic Water endmembers. This mixing of properties extends out to the slope, as highlighted by the overlain slope properties in Figure 7. In winter, water properties over the slope transition between the two described regimes: at depth, the water is temperature stratified, while it is purely salinity stratified above, just as the shelf is year-round. In the remaining seasons, the slope is temperature stratified throughout the water column. In sum, slope properties are most similar to shelf properties in winter, lying along straight mixing lines between shelf and offshore waters in T/S space.

We find that the waters in the core of the slope current (CF5 and CF6) are freshest and coldest in winter (Figure 8). Following their transformation in T/S space from fall to winter reveals that waters at a fixed depth level become denser through cooling, and also fresher, likely because surface cooling mixes down near-surface fresh water. Because the shallowest moored instruments are at 50 m, we do not measure the

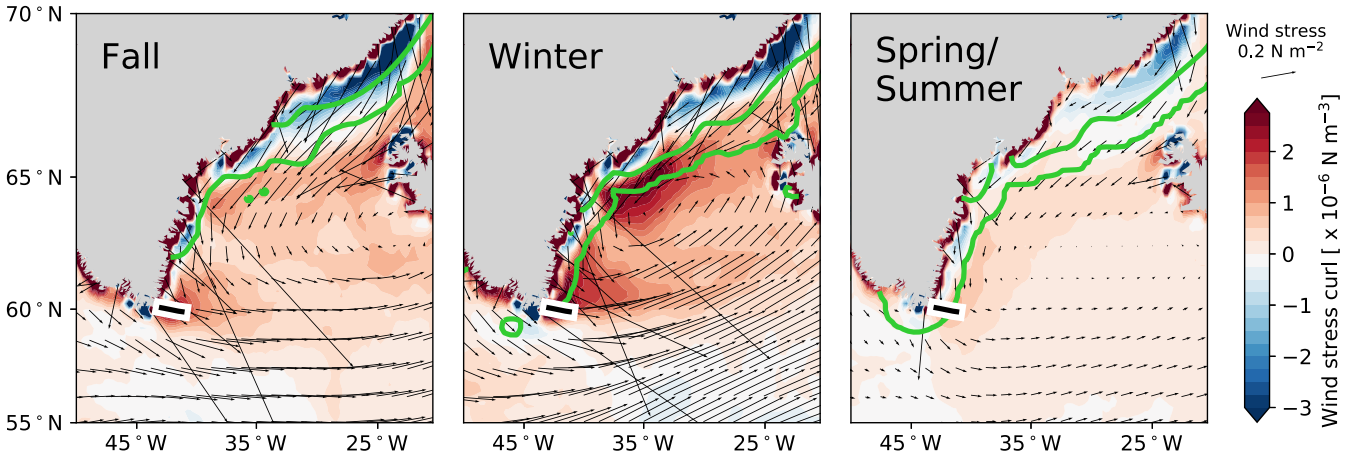

Figure 9. Wind stress curl from ERA5 wind stress fields during the three periods denoted in Figure 5 in the first year of measurements. Red and blue contours show wind stress curl, and arrows denote wind stress strength and direction for every fifth data point in *x* and *y*. The black line just southeast of Greenland indicates the position of the moored array. Thick green lines are the ERA5 sea ice concentration contours 0 and 0.2 in each period.

freshest water near the surface. However, from shipboard CTD profiles, we know that the water at the surface can be significantly fresher than it is at 50 m, providing a source of fresh water (see Appendix A). The properties we observe at CF in winter are likely the result of fresh water being mixed into the water column through cooling all along the eastern margin of Greenland, not only locally.

By the spring/summer, the water over the slope becomes warmer and saltier without a major change in density, suggesting isopycnal mixing (Figure 8). This transformation could also be due to a change in the properties which are advected in, or a shift in the position of the core of Atlantic Water, for example. Moving back to fall, the waters in the core of the slope current become lighter again as they warm.

3.5. Drivers of Volume Transport Variability

In this section, we consider the potential drivers of volume transport variability in the coastal and slope currents. We hypothesize that the volume transport variability we observe is primarily wind driven and test this by correlating volume transports with European Centre for Medium-Range Weather Forecasts ERA5 daily wind stress fields (Dee et al., 2011). The persistent wind features in this region are northerly along-coast winds and positive wind stress curl over the Irminger Basin (Figure 9). We correlate coastal and slope current volume transports with both along-stream wind stress (i.e., in the direction of the volume transport we report) and wind stress curl (Figure 10). The correlations are all at zero lag, but we apply a 5-day low-pass Butterworth filter to all time series before correlating them, so that an adjustment timescale of 5 days or less is implicit.

To identify the significance of the correlations in each case, we apply the FDR method, which is appropriate for diagnosing the collective significance of multiple hypothesis tests (Wilks, 2016). This is the case here because we correlate the transport at the array with the wind stress (curl) at many locations. We first convert all Pearson correlations (r) to t values using the equation: $t = r/\sqrt{(1-r^2)/(N_{\text{eff}})}$, where N_{eff} is the effective degrees of freedom (see section 2.2). These t values are converted to two-sided p values using a survival function. The p values are then sorted, and the highest significant p value is the maximum p value for which $p_i \leq (i/N)\alpha_{\text{FDR}}$, where i is the rank of the sorted p value and N is the total number of p values. We choose $\alpha_{\text{FDR}} = 0.1$, which means that the expected rate of false discovery is 10%. The corresponding minimum significant correlation coefficients found using this method are between 0.27 and 0.44, as reflected by the stippling in Figure 10.

The slope current volume transport's variability is significantly correlated with the wind stress curl over the Irminger Sea (Figure 10d). The correlation pattern is very similar to that found by Daniault, Lherminier, et al. (2011) and can be explained through gyre dynamics. Increased wind stress curl leads to Ekman divergence over the basin, upwelling of isopycnals in the center of the basin and the steepening of isopycnals at the basin boundaries, that is, in the slope current.

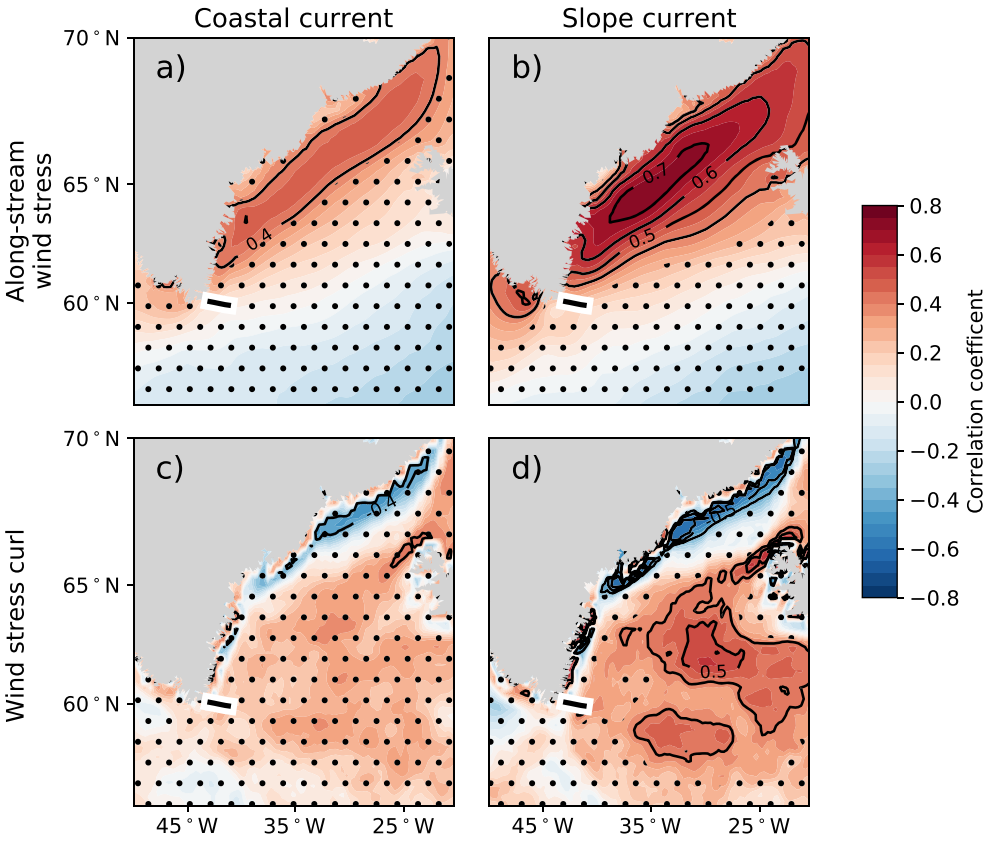

Figure 10. The correlation between combinations of (a and c) the coastal current volume transport and (b and d) slope current volume transport and the ERA5 (a and b) along-stream wind stress and (c and d) wind stress curl. The black line just southeast of Greenland indicates the position of our moored array. All time series are low-pass filtered with a 5-day cutoff frequency. Stippling indicates areas that are not significant using a 10% false discovery rate (see text).

The slope current's volume transport is even more significantly correlated with the along-stream wind stress over a large spatial scale: extending from Denmark Strait to Cape Farewell and from the Greenlandic coast to beyond the shelf area (Figure 10b). This correlation could be an artifact of the slope current's correlation with the wind stress curl, as the along-stream wind stress is a component of the wind stress curl. The pattern shows that the correlation with the wind stress curl is dominated by variability in wind stress along the coast.

We find that the coastal current's volume transport is correlated with along-stream wind stress on the shelf just upstream of the array (Figure 10a). This is consistent with a forcing mechanism discussed in Sutherland and Pickart (2008), Harden et al. (2014), and Bacon et al. (2014): northerly along-coast winds cause downwelling, which steepens isopycnals and hence accelerates the current through geostrophy. Unlike the slope current, the coastal current is not significantly correlated with wind stress curl over the basin (Figure 10c).

The correlation coefficients between the wind stress and coastal current transports are smaller than the correlation coefficients with the slope current transports, and the coastal current volume transport is not significantly correlated with along-stream wind stress at the moored array site. One possible explanation for this is that the upstream wind forcing is communicated southward by coastal trapped waves (Smith, 1978). The lack of correlation with local winds may also be due to uncertainty in the wind stress on the shelf due to the resolution of the ERA5 product (30 km) and/or to the effect of sea ice. Monthly estimates of sea ice derived from passive microwave satellite measurements indicate that sea ice is advected southward along the east coast of Greenland, rarely rounding the tip of CF (Figure 11). Sea ice is confined to the shelf, which could account for part of the difference in coastal and slope current forcing. Sea ice can change the direction of the ocean's Ekman response to the wind (Cole et al., 2014), potentially slowing the component of the coastal current in the along-stream direction when more sea ice is present. Sea ice concentration peaks in April/May during our observation years, when the coastal current is the slowest, lending some support to this idea. At the same

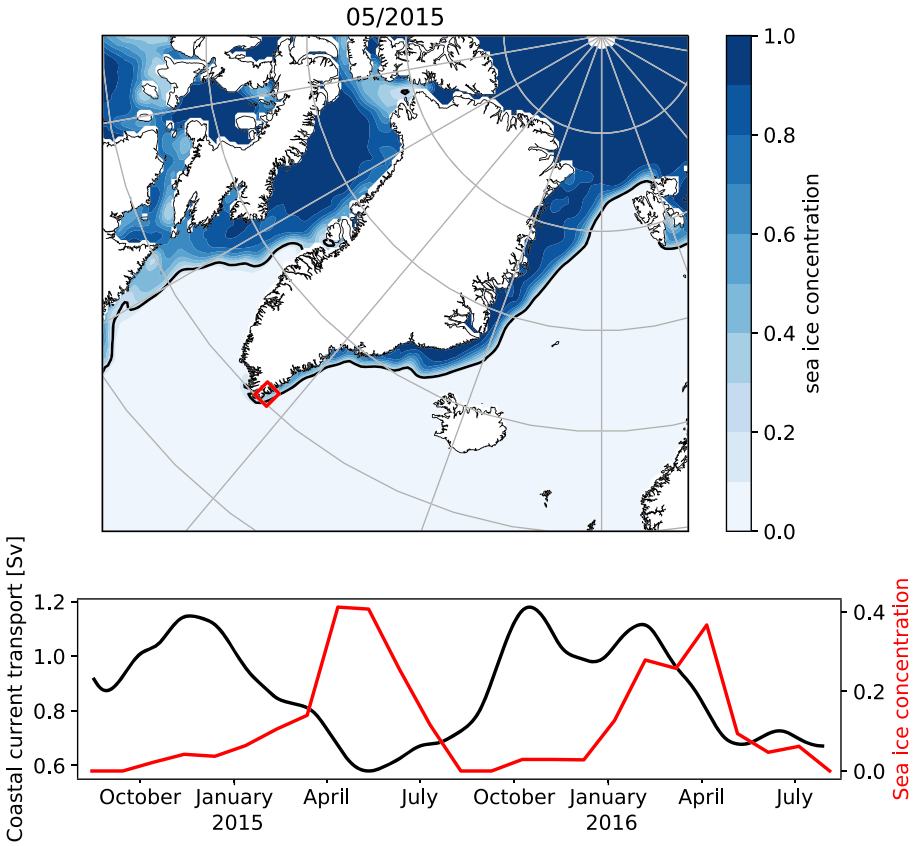

Figure 11. (top) Sea ice concentration from National Snow and Ice Data Center passive microwave brightness temperature data in May 2015, which had the maximum sea ice concentration over our array. The black contour is the 0.2 sea ice concentration contour, and the red box shows the area over which sea ice concentration was averaged in bottom panel. (bottom) Sea ice concentration on the shelf over the moored array (red, right axis) and coastal current volume transport (black, left axis).

time, mobile ice pack tends to enhance momentum transfer into the ocean, which is not consistent with what we observe (Schulze & Pickart, 2012).

Another possible explanation for the covariability of the sea ice concentration and coastal current volume transport is that the slowing of the coastal current leads to a convergence in sea ice at CF in spring before air temperatures rise above the melting point of sea ice. This would account for the sea ice maximum as the coastal current slows. As the seasonality we observe in coastal current freshwater transport is dominated by velocity fluctuations, we do not think that local sea ice melt drives freshwater transport seasonality during our sampling period.

In sum, we find that the coastal current and slope current volume transport variabilities are consistent with hypothesized wind forcing mechanisms and find a potential role for buoyancy forcing and sea ice. The coastal current accelerates in late fall, when density gradients are largest and downwelling-favorable winds steepen isopycnals, increasing geostrophic velocity. The slope current transport responds to wind stress curl over the Irminger Sea via gyre-scale dynamics. Simultaneously, isopycnals and isohalines deepen due to winter cooling, decreasing the salinity of the slope current (section 3.4) and decreasing isopycnal gradients on the shelf (Figure 6), which could decelerate the coastal current. The coastal current may also slow in winter due to sea ice, which affects the transfer of momentum from wind stress into the ocean on the shelf.

4. Discussion

Eight OSNAP moorings southeast of Greenland reveal two distinct, persistent currents on the continental shelf and slope from August 2014 to August 2016. These are the first year-round observations of freshwater

transport in the EGC system south of Fram Strait, and we find that the coastal and slope currents combined account for 70% of the total freshwater transport across the eastern subpolar gyre. The remaining freshwater transport across the line is accounted for by the Deep Western Boundary Current and northward flowing salty waters of Atlantic origin.

The freshwater transport is partitioned approximately equally between the coastal current (EGCC; 42 ± 6 mSv) and the fresh portion of the slope current (EGC; 32 ± 6 mSv)in our measurement years. Coastal current freshwater transport almost doubles from June to December (28 to 57 mSv), and the EGC quadruples from August to February (12 to 51 mSv). This suggests that summer shipboard measurements may be significantly underestimating freshwater transport in this region and that the role of the EGC on the shelfbreak has been particularly underestimated. Sutherland and Pickart (2008) found that the EGCC carried two times as much freshwater transport as the EGC from one summer snapshot at 60° N, while our results point to a more equal partitioning over the course of the year. We also observe a significant amount of variability in our daily transport estimates (Figures 3 and 4), further calling the representative nature of synoptic measurements into question.

Improved understanding of the temporal and spatial distribution of freshwater on the shelf and slope east of Greenland is of particular importance because it has the potential to disrupt convection if it enters the interior of the subpolar gyre. Several regions where freshwater deviates into the interior have been identified downstream of our array in observations: the tip of CF (Holliday et al., 2007) and the unstable West Greenland Current (Bracco et al., 2008; Myers et al., 2009; Rykova et al., 2015; Schmidt & Send, 2007). Furthermore, several recent modeling studies have found that freshwater originating east of Greenland is more likely to enter the Labrador Sea than freshwater originating west of Greenland (Gillard et al., 2016; Luo et al., 2016; Marson et al., 2018; Tesdal et al., 2018; Wang et al., 2018). In particular, water over the slope east of Greenland is more likely to enter the Labrador Sea than water originating on the shelf (Schulze Chretien & Frajka-Williams, 2018).

So, though fresher waters are found on the shelf year-round (Figure 7), freshening over the slope will likely have a greater impact on convection. Hence, the minimum in salinity we find over the slope in winter is of particular interest (Figure 6). We hypothesize that this wintertime freshwater maximum over the slope is caused by wintertime cooling, which mixes freshwater into the water column. The water properties over the slope are well-represented by mixing between a shelf endmember and offshore waters (Figure 7), indicating that the shelf is potentially the source of the anomalously fresh waters over the slope in winter. It is also worth noting that the freshwater over the slope is only tens of kilometers from deep convection sites in the Irminger Sea (Våge et al., 2011), and the maximum in freshwater over the slope is concurrent with convection there. Another consideration is that the downwelling of mass in the Atlantic Meridional Overturning Circulation actually occurs at the margins of the subpolar gyre (Brüggeman et al., 2017; Katsman et al., 2018; Spall, 2010; Spall & Pickart, 2001; Straneo, 2006). In this view, the properties over the slope could be subducted directly and imprint the lower limb of the overturning circulation beyond interaction with deep convection.

Diagnosing the drivers of variability in the EGC system is a critical first step to understanding freshwater distribution in the subpolar North Atlantic. We find that the volume transport variability in the coastal and slope currents is consistent with wind-driven mechanisms (Figure 10). Variability in the slope current appears to be driven by large-scale wind stress curl over the Irminger Basin, as found by Daniault, Lherminier, et al. (2011). The coastal current responds to increased downwelling-favorable along-stream wind stress in the fall, which steepen isopycnals on the shelf and accelerate the current through geostrophy, as hypothesized by Sutherland and Pickart (2008). The reason that the coastal current slows in winter is less clear. One hypothesis is that the arrival of sea ice affects the response of the shelf waters to the wind (Figure 11). Another possible explanation is that horizontal density gradients are decreased in winter by cooling (Bacon et al., 2014).

Our results provide a new benchmark for models to test whether they reproduce the integrated effect of all freshwater inputs on the shelves. Models have been moving to increasingly high-resolution and realistic freshwater forcing from Greenland; even icebergs are beginning to be included realistically (Marson et al., 2018). Resolution has been found to be critical to mapping freshwater pathways into convective regions (Dukhovskoy et al., 2016; Gillard et al., 2016; Luo et al., 2016), and new insights are being gained into the magnitude of the effect of freshwater forcing on convection and the overturning circulation. Lenaerts et al. (2015) predict that rising temperatures will have a greater impact on the overturning circulation than increased runoff from Greenland. Böning et al. (2016) found a relatively muted decrease in deep convection due to increased meltwater from Greenland using a high-resolution, global ocean-sea ice coupled model from 1990 to 2020. Most models are using seasonally and interannually varying runoff forcing from Greenland at the

surface of the most coastal grid cell, which is a significant step toward realism from traditional hosing experiments. At the same time, we find that the timing of maximum freshwater and freshwater export on the shelf (December) does not align with the freshwater pulse from seasonal melt in Greenland (August). This may be due to delays in export from glaciers to fjords to the shelf, control by wind-driven transport divergence on the shelf, or dominance of Arctic origin freshwater. Regardless of the cause, replication of the freshwater distribution on the shelf and slope and its variability as observed by OSNAP is a new and perhaps more relevant metric which is available for model studies examining the effect of freshwater on convection as they continue to approach reality.

We do not calculate solid freshwater transport across our line, but Bacon et al. (2014) use a model to estimate an annual mean solid (sea ice) freshwater flux of 13 mSv at CF (referenced to 34.8), which is 15% of the total freshwater transport they report at CF. The seasonality in solid freshwater flux in Bacon et al. (2014) reflects the sea ice concentration we show in Figure 11. The proportion of liquid to solid freshwater transport increases from Fram Strait to Cape Farewell as sea ice melts along the way. At Fram Strait, the liquid and solid portions of the freshwater transport are approximately equal: de Steur et al. (2009) report a 10-year mean liquid freshwater transport of 66 mSv from 1998 to 2008, and Kwok et al. (2004) estimate a 24-year mean sea ice freshwater transport of 70 mSv from 1978 to 2002, both referenced to 34.9 as in our study.

The total mean freshwater transport through Fram Strait, 136 mSv, greatly exceeds our estimates at Cape Farewell. Havik et al. (2017) report on summer 2012 shipboard measurements of the EGC system as it evolves from Fram Srait to Denmark Strait. They find that freshwater transport decreases along the way and estimates 81 ± 8 mSv of freshwater transport referenced to 34.8 just north of the Denmark Strait at their section 3. At Denmark Strait, de Steur et al. (2016) report an 11-month average liquid (2011–2012) freshwater transport of 84 mSv referenced to 34.8 but do not estimate solid freshwater transport. The de Steur et al. (2016) measurements coincided with an anomalously fresh summer, and they highlight the importance of comparing freshwater transports at similar time periods. The decrease in freshwater transport from Fram Strait to Denmark Strait is likely due to freshwater diversion into the Nordic Seas: Dodd et al. (2009) estimate that 49 mSv of sea ice and 15 mSv of liquid freshwater transport (referenced to 34.8) are diverted into the Nordic Seas at this point.

The freshwater transports reported by Havik et al. (2017) and de Steur et al. (2016) in the vicinity of Denmark Strait are very similar to the mean liquid freshwater transport we measure at Cape Farewell: 77 mSv of waters fresher than 34.9. We might expect our estimate to be larger, as additional freshwater from Greenland's melting glaciers has been added. This may be due to the fact that even with three moorings on the shelf, we are barely resolving the coastal current, and surface and inner shelf salinities are underresolved (Appendix A). Alternately, there may be freshwater fluxes into the interior that are replaced by additional freshwater from Greenland.

Our results indicate that local wind stress forcing dominates over the propagation of freshwater transport seasonality along eastern Greenland. Harden et al. (2014) find a maximum in EGCC freshwater transport from January to April just south of Sermilik Fjord, at about 65° N. Their estimates are consistent with the timing and amount of freshwater advected from the Arctic through Fram Strait; however, the reported peak in freshwater at 65° N is later than the one we find in the coastal current at Cape Farewell. Additionally, transport seasonality at Fram Strait has been found to be dependent on measurement position, indicating the importance of local wind stress forcing there as well (de Steur et al., 2014).

The seasonality in water mass properties we find is consistent with the seasonality downstream of our array to the extent that it is known. Rykova et al. (2015) characterized the seasonality of transports and water mass properties west of Greenland, where cold, fresh water sits atop warm, salty water in the IC. They found that the subsurface salinity/temperature maximum is the largest in winter (October–February), while the surface freshwater portion is strongest in summer (May–July). de Jong et al. (2014) found similar patterns in Irminger Rings shed from the West Greenland Current: the warmest and saltiest eddies were observed in the fall and freshwater caps were observed in spring. This seasonality is consistent with a several month propagation time from our array (Grist et al., 2014; Schmidt & Send, 2007), as we find the warmest and saltiest water in early fall and maximum freshwater transports in late fall/winter. However, the seasonality west of Greenland is only known to within several months due to the dearth of observations outside of summer, and both components of the West Greenland Current are known to exhibit strong interannual variability (Myers et al., 2007, 2009).

Table A1
Summertime Coastal Current (East Greenland Coastal Current) Volume and Freshwater Transports From OSNAP Shipboard Observations and Cape Farewell Moorings,

		Volume transport (Sv)	Freshwater transport (mSv)
OSNAP cruises	August 2014	0.9	52
	July 2016	0.9	37
OSNAP moorings (monthly mean and range)	August 2014	0.7 (0.2–1.1)	34 (11–60)
	July 2016	0.6 (0.1–1.0)	28 (5–49)

Note. OSNAP = Overturning in the Subpolar North Atlantic Program.

The continuation of OSNAP will allow us to assess how representative the seasonality we have observed so far is and identify its forcing mechanisms with greater confidence. This will be particularly interesting because there were large negative heat fluxes over the Irminger Sea in the winters of 2015 and 2016 (de Jong & de Steur, 2016). These anomalously cold temperatures may have been responsible for the previously unmeasured freshwater content peak at 100–300 m we find over the continental slope in winter. Moving forward, we hope to understand what governs the formation of this winter freshwater content peak and how it interacts with convection downstream.

Appendix A: Comparison With Shipboard Coastal Current Measurements

The slope current is wider than the distance between our moorings, so that it is well resolved by the array. However, the coastal current is not as well resolved because its core is only measured by the CF1 mooring. A comparison with the shipboard measurements taken on the mooring deployment and recovery cruises adds insight into the error due to the portions of the current we miss.

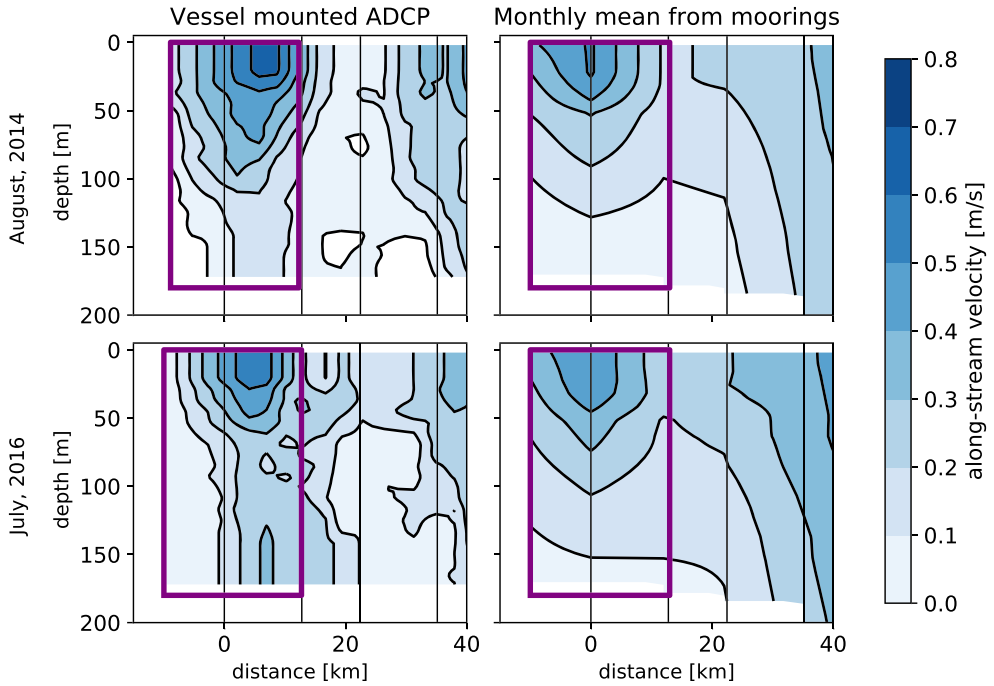

Figure A1. Along-stream velocity measured by vessel mounted ADCP on mooring deployment and recovery cruises (left) and monthly averages from the moored array during the first and last months of the deployment (right). Purple rectangles indicate the area used to calculate the volume and freshwater transports quoted in Table A1, which was held constant across data sources. Black vertical lines indicate Cape Farewell mooring positions. ADCP = Acoustic Doppler Current Profiler.

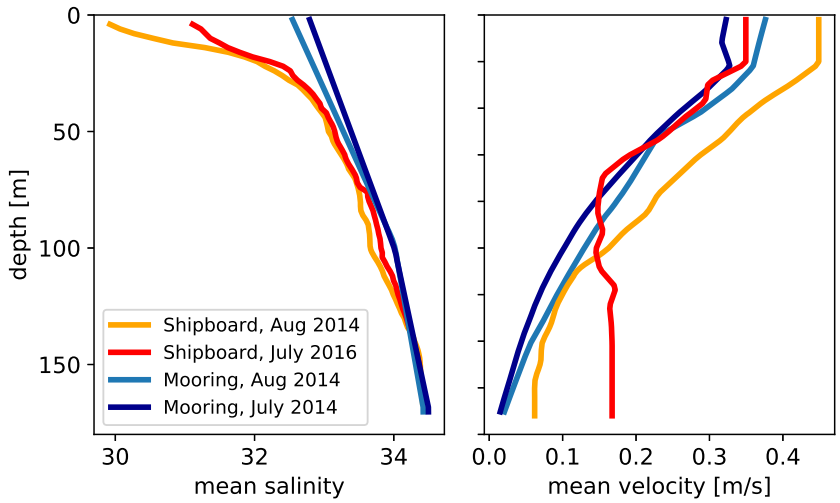

Figure A2. Mean salinity and velocity profiles within the coastal current (purple rectangle in Figure A1) from shipboard vessel mounted Acoustic Doppler Current Profiler and CTD measurements and monthly averages estimated from the moored array.

As described in Lin et al. (2018), the shipboard CTD thermistors were calibrated in the laboratory precruise and postcruise; conductivity sensors were calibrated using CTD rosette water samples, yielding a temperature accuracy of 0.001 °C and 0.002 for salinity. Vessel-mounted ADCP velocity measurements were processed using the Common Ocean Data Access System, heading corrected, and de-tided using a barotropic tidal model after Egbert and Erofeeva (2002). They estimate an ADCP velocity uncertainty of 0.02–0.03 m/s. For further details, the reader is referred to Lin et al. (2018).

Transports are calculated using the same portion of the shelf. Note that the August 2014 section shipboard section used (k2) is just upstream of the moored array (Lin et al., 2018). Shipboard transport estimates as well as monthly means and ranges from the moored array are listed in Table A1.

The shipboard volume transport is underestimated by the moored estimate because the velocity maximum is offset from the CF1 mooring as measured by the vessel mounted ADCP (Figure A1). The freshwater transport is underestimated through a nonlinear combination of underestimating the velocity and overestimating the surface salinity (Figure A2), with both contributing approximately equally to the discrepancy.

The volume and freshwater transports estimated using shipboard data fall within the range measured by the moorings over 1 month, indicating large synoptic variability and/or that the current core passes through CF1 periodically.

The lack of surface salinity measurements contributes to the underestimation of coastal current freshwater transports in the summer and likely in the fall. As the near-surface stratification weakens in the winter, though, this bias is likely less significant. This could affect the observed seasonality in freshwater transport, though the seasonal range observed (30 mSv, conservatively) is larger than the underestimation of freshwater transport by the moored array (10–20 mSv). Further, the observed seasonality in the coastal current is due to variations in velocity, which are likely to be biased consistently throughout the year. In sum, while the coastal current transports are likely underestimated by our array, the observed seasonality is a robust pattern.

Acknowledgments
We gratefully acknowledge the U.S. National Science Foundation: this work was supported by grant OCE-1258823. N. P. H. was supported by NERC programmes UK OSNAP (NE/K010875) and ACSIS (National Capability). All U.S. OSNAP mooring data can be found at http://www.o-snap.org/observations/data/. The U.S. Cape Farewell portion reported on here is available from doi:10.7924/r4fb50z9b. The U.K. data are available from bodc.ac.uk and at https://doi.org/10.5285/6cb6dc0c-7bed-3ca4-e053-6c86abc0b9f0. We thank two anonymous reviewers, whose comments led to significant improvements. We thank F. Li and M. S. Lozier for providing the mean salinity across the OSNAP East line. The data presented in this manuscript would not have come about without the hard work of the entire OSNAP team, especially all scientists, technical staff, and crew who went to sea to collect this data. In particular, we thank A. Ramsey, F. Bahr, D. Torres, R. Pickart, P. Lin, A. Pacini, J. Ryder, J. Kemp, B. Hogue, and A. Davies.

References

Aagaard, K., & Carmack, E. C. (1989). The role of sea ice and other fresh water in the Arctic circulation. *Journal of Geophysical Research*, *94*, 14485.

Alley, R. B., Clark, P. U., Huybrechts, P., & Joughin, I. (2005). Ice-sheet and sea-level changes. *Science (New York, N.Y.)*, *310*, 456–60.

Bacon, S., Aksenov, Y., Fawcett, S., & Madec, G. (2015). Arctic mass, freshwater and heat fluxes: Methods and modelled seasonal variability. *Philosophical Transactions of the Royal Society A: Mathematical Physical and Engineering Sciences*, *373*, 20140169.

Bacon, S., Marshall, A., & Holliday, N. P. (2014). Seasonal variability of the East Greenland Coastal Current. *Journal of Geophysical Research: Oceans*, *119*, 3967–3987. https://doi.org/10.1002/2013JC009279

Bacon, S., Myers, P. G., Rudels, B., & Sutherland, D. A. (2008). Accessing the inaccessible: Buoyancy-driven coastal currents on the shelves of Greenland and Eastern Canada. In R. R. Dickson, J. Meincke, & P. Rhines (Eds.), *Arctic subarctic ocean fluxes: Defining the role of the Northern Seas in climate* (chap. 28, pp. 703–722). Berlin: Springer.

Bacon, S., Reverdin, G., Rigor, I. G., & Snaith, H. M. (2002). A freshwater jet on the east Greenland shelf. *Journal of Geophysical Research*, *107*, 5.1–5.16.

Bacon, S., & Saunders, P. M. (2010). The deep western boundary current at Cape Farewell: Results from a moored current meter array. *Journal of Physical Oceanography*, *40*, 815–829.

Böning, C. W., Behrens, E., Biastoch, A., Getzlaff, K., & Bamber, J. L. (2016). Emerging impact of Greenland meltwater on deepwater formation in the North Atlantic Ocean. *Nature Geoscience*, *9*, 523–527.

Bracco, A., Pedlosky, J., & Pickart, R. S. (2008). Eddy formation near the west coast of Greenland. *Journal of Physical Oceanography*, *38*, 1992–2002.

Brüggeman, N., Katsman, C. A., & Dijkstra, H. A. (2017). On the vorticity dynamics of the downwelling branch of the AMOC. *CLIVAR Exchanges Special Issue: CLIVAR Open Science Conference Award Winners*, *71*, 10–12.

Cole, S. T., Timmermans, M.-L., Toole, J. M., Krishfield, R. A., & Veering, F. T. Thwaites. (2014). Ekman internal waves, and turbulence observed under Arctic sea ice. *Journal of Physical Oceanography*, *44*, 1306–1328.

Cox, K. A., Stanford, J. D., McVicar, A. J., Rohling, E. J., Heywood, K. J., Bacon, S., et al. (2010). Interannual variability of Arctic sea ice export into the East Greenland Current. *Journal of Geophysical Research*, *115*, C12063. https://doi.org/10.1029/2010JC006227

Daniault, N., Lherminier, P., & Mercier, H. (2011). Circulation and transport at the southeast tip of Greenland. *Journal of Physical Oceanography*, *41*, 437–457.

Daniault, N., Mercier, H., & Lherminier, P. (2011). The 1992–2009 transport variability of the East Greenland-Irminger Current at 60°N. *Geophysical Research Letters*, *38*, L07601. https://doi.org/10.1029/2011GL046863

de Jong, M. F., Bower, A. S., & Furey, H. H. (2014). Two years of observations of warm-core anticyclones in the Labrador Sea and their seasonal cycle in heat and salt stratification. *Journal of Physical Oceanography*, *44*, 427–444.

de Jong, M. F., & de Steur, L. (2016). Strong winter cooling over the Irminger Sea in winter 2014–2015, exceptional deep convection, and the emergence of anomalously low SST. *Geophysical Research Letters*, *43*, 7106–7113. https://doi.org/10.1002/2016GL069596

de Steur, L., Hansen, E., Gerdes, R., Karcher, M., Fahrbach, E., & Holfort, J. (2009). Freshwater fluxes in the East Greenland Current: A decade of observations. *Geophysical Research Letters*, *36*, L23611. https://doi.org/10.1029/2009GL041278

de Steur, L., Hansen, E., Mauritzen, C., Beszczynska-möller, A., & Fahrbach, E. (2014). Impact of recirculation on the East Greenland Current in Fram Strait: Results from moored current meter measurements between 1997 and 2009. *Deep-Sea Research Part*, *I*(92), 26–40.

de Steur, L., Pickart, R. S., Macrander, A., Våge, K., Harden, B. E., Jonsson, S., et al. (2016). Liquid freshwater transport estimates from the East Greenland Current based on continuousmeasurements north of Denmark Strait. *Journal of Geophysical Research: Oceans*, *122*, 93–109. https://doi.org/10.1002/2016JC012106

Dee, D. P., Uppala, S. M., Simmons, A. J., Berrisford, P., Poli, P., Kobayashi, S., et al. (2011). The ERA5 reanalysis: Configuration and performance of the data assimilation system. *Quarterly Journal of the Royal Meteorological Society*, *137*, 553–597.

Dodd, P. A., Heywood, K. J., Meredith, M. P., Naveira-Garabato, A. C., Marca, A. D., & Falkner, K. K. (2009). Sources and fate of freshwater exported in the East Greenland Current. *Geophysical Research Letters*, *36*, L19608. https://doi.org/10.1029/2009GL039663

Dukhovskoy, D. S., Myers, P. G., Platov, G., Timmermans, M., Curry, B., Proshutinsky, A., et al. (2016). Greenland freshwater pathways in the sub-Arctic Seas from model experiments with passive tracers. *Journal of Geophysical Research: Oceans*, *121*, 877–907. https://doi.org/10.1002/2015JC011290

Egbert, G. D., & Erofeeva, S. Y. (2002). Efficient inverse modeling of barotropic ocean tides. *Journal of Atmospheric and Oceanic Technology*, *19*, 183–204.

Gillard, L. C., Hu, X., Myers, P. G., & Bamber, J. L. (2016). Meltwater pathways from marine terminating glaciers of the Greenland ice sheet. *Geophysical Research Letters*, *43*, 10873–10882. https://doi.org/10.1002/2016GL070969

Grist, J. P., Josey, S. A., Boehme, L., Meredith, M. P., Laidre, K. L., Heide-Jørgensen, M. P., et al. (2014). Seasonal variability of the warm Atlantic water layer in the vicinity of the Greenland shelf break. *Geophysical Research Letters*, *41*, 8530–8537. https://doi.org/10.1002/2014GL062051

Harden, B. E., Straneo, F., & Sutherland, D. A. (2014). Moored observations of synoptic and seasonal variability in the East Greenland Coastal Current. *Journal of Geophysical Research: Oceans*, *119*, 8838–8857. https://doi.org/10.1002/2014JC010134

Havik, L., Pickart, R. S., Torres, D. J., Thurnherr, A. M., Beszczynska-Möller, A., Walczowki, W., & von Appen, W.-J. (2017). Evolution of the East Greenland Current from Fram Strait to Denmark Strait synoptic measurements from summer 2012. *Journal of Geophysical Research: Oceans*, *122*, 1974–1994. https://doi.org/10.1002/2016JC012228

Holliday, N. P., Bacon, S., Cunningham, S. A., Gary, S. F., Karstensen, J., King, B. A., et al. (2018). Subpolar North Atlantic overturning and gyre-scale circulation in the summers of 2014 and 2016. *Journal of Geophysical Research: Oceans*, *123*, 4538–4559. https://doi.org/10.1029/2018JC013841

Holliday, N. P., Meyer, A., Bacon, S., Alderson, S. G., & de Cuevas, B. (2007). Retroflection of part of the east Greenland current at Cape Farewell. *Geophysical Research Letters*, *34*, L07609. https://doi.org/10.1029/2006GL029085

Kanzow, T., Send, U., Zenk, W., Chave, A. D., & Rhein, M. (2006). Monitoring the integrated deep meridional flow in the tropical North Atlantic: Long-term performance of a geostrophic array. *Deep-Sea Research*, *I*(53), 528–546.

Katsman, C. A., Drijfhout, S. S., Dijkstra, H. A., & Spall, M. A. (2018). Sinking of dense North Atlantic waters in a global ocean model location and controls. *Journal of Geophysical Research: Oceans*, *123*, 3563–3576. https://doi.org/10.1029/2017JC013329

Kwok, R., Cunningham, G. F., & Pang, S. S. (2004). Fram Strait sea ice outflow. *Journal of Geophysical Research*, *109*, C01009. https://doi.org/10.1029/2003JC001785

Lavender, K. L., Brechner Owens, W., & Davis, R. E. (2005). The mid-depth circulation of the subpolar North Atlantic Ocean as measured by subsurface floats. *Deep Sea Research Part I: Oceanographic Research Papers*, *52*, 767–785.

Lazier, J. R. (1980). Oceanographic conditions at Ocean Weather Ship Bravo, 1964–1974. *Atmosphere-Ocean*, *18*, 227–238.

Lenaerts, J. T. M., Le Bars, D., Van Kampenhout, L., Vizcaino, M., Enderlin, E. M., & Van Den Broeke, M. R. (2015). Representing Greenland ice sheet freshwater fluxes in climate models. *Geophysical Research Letters*, *42*, 6373–6381. https://doi.org/10.1002/2015GL064738

Lherminier, P., Mercier, H., Huck, T., Gourcuff, C., Perez, F. F., Morin, P., et al. (2010). The Atlantic Meridional Overturning Circulation and the subpolar gyre observed at the A25-OVIDE section in June 2002 and 2004. *Deep Sea Research Part I: Oceanographic Research Papers*, *57*, 1374–1391.

Li, F., Lozier, M. S., & Johns, W. E. (2017). Calculating the meridional volume, heat, and freshwater transports from an observing system in the subpolar North Atlantic: Observing system simulation experiment. *Journal of Atmospheric and Oceanic Technology*, *34*, 1483–1500.

Lilly, J. M., Rhines, P. B., Schott, F., Lavender, K., Lazier, J., Send, U., & D'Asaro, E. (2003). Observations of the Labrador Sea eddy field. *Progress in Oceanography*, *59*, 75–176.

Lin, P., Pickart, R. S., Torres, D. J., Pacini, A., Lin, P., Pickart, R. S., et al. (2018). Evolution of the freshwater coastal current at the southern tip of Greenland. *Journal of Physical Oceanography*, *48*, 2127–2140.

Lozier, M. S., Bacon, S., Bower, A. S., Cunningham, S. A., Femke de Jong, M., de Steur, L., et al. (2017). Overturning in the subpolar North Atlantic Program: A new international ocean observing system. *Bulletin of the American Meteorological Society*, *98*, 737–752.
Luo, H., Castelao, R. M., Rennermalm, A. K., Tedesco, M., Bracco, A., Yager, P., & Mote, T. L. (2016). Oceanic transport of surface meltwater from the southern Greenland ice sheet. *Nature Geoscience*, *9*, 528–532.
Manabe, S., & Stouffer, R. J. (1995). Simulation of abrupt climate change induced by freshwater input to the North Atlantic Ocean. *Nature*, *378*, 165–167.
Marson, J. M., Myers, P. G., Hu, X., & Le Sommer, J. (2018). Using vertically integrated ocean fields to characterize Greenland icebergs' distribution and lifetime. *Geophysical Research Letters*, *45*, 4208–4217. https://doi.org/10.1029/2018GL077676
Myers, P. G., Donnelly, C., & Ribergaard, M. H. (2009). Structure and variability of the West Greenland Current in summer derived from 6 repeat standard sections. *Progress in Oceanography*, *80*, 93–112.
Myers, P. G., Kulan, N., & Ribergaard, M. H. (2007). Irminger water variability in the West Greenland Current. *Geophysical Research Letters*, *34*, L17601. https://doi.org/10.1029/2007GL030419
Pickart, R. S., Torres, D. J., & Fratantoni, P. S. (2005). The East Greenland spill jet. *Journal of Physical Oceanography*, *35*, 1037–1053.
Rossby, T., Reverdin, G., Chafik, L., & Søiland, H. (2017). A direct estimate of poleward volume, heat, and freshwater fluxes at 59.5° N between Greenland and Scotland. *Journal of Geophysical Research: Oceans*, *122*, 5870–5887. https://doi.org/10.1002/2017JC012835
Rudels, B., Björk, G., Nilsson, J., Winsor, P., Lake, I., & Nohr, C. (2005). The interaction between waters from the Arctic Ocean and the Nordic Seas north of Fram Strait and along the East Greenland Current: Results from the Arctic Ocean-02 Oden expedition. *Journal of Marine Systems*, *55*, 1–30.
Rykova, T., Straneo, F., & Bower, A. S. (2015). Seasonal and interannual variability of the West Greenland Current System in the Labrador Sea in 1993–2008. *Journal of Geophysical Research: Oceans*, *120*, 1318–1332. https://doi.org/10.1002/2014JC010386
Sarafanov, A., Falina, A., Mercier, H., Sokov, A., Lherminier, P., Gourcuff, C., et al. (2012). Mean full-depth summer circulation and transports at the northern periphery of the Atlantic Ocean in the 2000s. *Journal of Geophysical Research*, *117*, C01014. https://doi.org/10.1029/2011JC007572
Schmidt, S., & Send, U. (2007). Origin and composition of seasonal Labrador Sea freshwater. *Journal of Physical Oceanography*, *37*, 1445–1454.
Schulze Chretien, L. M., & Frajka-Williams, E. (2018). Wind-driven transport of fresh shelf water into the upper 30 m of the Labrador Sea. *Ocean Science*, *14*, 1247–1264.
Schulze, L. M., & Pickart, R. S. (2012). Seasonal variation of upwelling in the Alaskan Beaufort Sea Impact of sea ice cover. *Journal of Geophysical Research*, *117*, C06022. https://doi.org/10.1029/2012JC007985
Smith, R. L. (1978). Poleward propagating perturbations in currents and sea levels along the Peru Coast. *Journal of Geophysical Research*, *83*, 6083.
Spall, M. A. (2010). Dynamics of downwelling in an eddy-resolving convective basin. *Journal of Physical Oceanography*, *40*, 2341–2347.
Spall, M. A., & Pickart, R. S. (2001). Where does dense water sink? A subpolar gyre example. *Journal of Physical Oceanography*, *31*, 810–826.
Spall, M. A., & Pickart, R. S. (2003). Wind-driven recirculations and exchange in the Labrador and Irminger Seas. *Journal of Physical Oceanography*, *33*, 1829–1845.
Straneo, F. (2006). On the connection between dense water formation, overturning, and poleward heat transport in a convective basin. *Journal of Physical Oceanography*, *36*, 1822–1840.
Straneo, F., Hamilton, G. S., Sutherland, D. A., Stearns, L. A., Davidson, F., Hammill, M. O., et al. (2010). Rapid circulation of warm subtropical waters in a major glacial fjord in East Greenland. *Nature Geoscience*, *3*, 182–186.
Sutherland, D. A., & Cenedese, C. (2009). Laboratory experiments on the interaction of a buoyant coastal current with a canyon application to the East Greenland Current. *Journal of Physical Oceanography*, *39*, 1258–1271.
Sutherland, D. A., & Pickart, R. S. (2008). The East Greenland coastal current: Structure, variability, and forcing. *Progress in Oceanography*, *78*, 58–77.
Sutherland, D. A., Pickart, R. S., Peter Jones, E., Azetsu-Scott, K., Jane Eert, A., & Ólafsson, J. (2009). Freshwater composition of the waters off southeast Greenland and their link to the Arctic Ocean. *Journal of Geophysical Research*, *114*, C05020. https://doi.org/10.1029/2008JC004808
Tesdal, J.-E., Abernathey, R. P., Goes, J. I., Gordon, A. L., & Haine, T. W. N. (2018). Salinity trends within the upper layers of the subpolar North Atlantic. *Journal of Climate*, *31*, 2675–2698.
Tsubouchi, T., Bacon, S., Naveira Garabato, A. C., Aksenov, Y., Laxon, S. W., Fahrbach, E., et al. (2012). The Arctic Ocean in summer: A quasi-synoptic inverse estimate of boundary fluxes and water mass transformation. *Journal of Geophysical Research*, *117*, C01024. https://doi.org/10.1029/2011JC007174
Våge, K., Pickart, R. S., Sarafanov, A., Knutsen, Ø., Mercier, H., Lherminier, P., et al. (2011). The Irminger Gyre: Circulation, convection, and interannual variability. *Deep-Sea Research Part I: Oceanographic Research Papers*, *58*, 590–614.
Wang, H., Legg, S., & Hallberg, R. (2018). The effect of Arctic freshwater pathways on North Atlantic Convection and the Atlantic Meridional Overturning Circulation. *Journal of Climate*, *31*, 5165–5188.
Wang, M., & Overland, J. E. (2009). A sea ice free summer Arctic within 30 years? *Geophysical Research Letters*, *36*, L07502. https://doi.org/10.1029/2009GL037820
Weijer, W., Maltrud, M. E., Hecht, M. W., Dijkstra, H. A., & Kliphuis, M. A. (2012). Response of the Atlantic Ocean circulation to Greenland Ice Sheet melting in a strongly-eddying ocean model. *Geophysical Research Letters*, *39*, L09606. https://doi.org/10.1029/2012GL051611,
Wilkinson, D., & Bacon, S. (2005). The spatial and temporal variability of the East Greenland Coastal Current from historic data. *Geophysical Research Letters*, *32*, L24618. https://doi.org/10.1029/2005GL024232
Wilks, D. S. (2016). The stippling shows statistically significant grid points. *BAMS*, *97*, 2263–2274.
Yang, Q., Dixon, T. H., Myers, P. G., Bonin, J., Chambers, D., van den Broeke, M. R., et al. (2016). Recent increases in Arctic freshwater flux affects Labrador Sea convection and Atlantic overturning circulation. *Nature Communications*, *7*, 10525.